frontiers | Frontiers in Astronomy and Space Sciences

TYPE Original Research
PUBLISHED 28 March 2024
DOI 10.3389/fspas.2024.1324796

Check for updates

OPEN ACCESS

EDITED BY
Renee Ludlam,
Wayne State University, United States

REVIEWED BY
Lijun Gou,
Chinese Academy of Sciences (CAS), China
Eilat Glikman,
Middlebury College, United States

*CORRESPONDENCE
J. M. Piotrowska,
✉ joannapk@caltech.edu

†CITA National Fellow

RECEIVED 20 October 2023
ACCEPTED 16 February 2024
PUBLISHED 28 March 2024

CITATION
Piotrowska JM, García JA, Walton DJ, Beckmann RS, Stern D, Ballantyne DR, Wilkins DR, Bianchi S, Boorman PG, Buchner J, Chen C-T, Coppi P, Dauser T, Fabian AC, Kammoun E, Madsen K, Mallick L, Matt G, Matzeu G, Nardini E, Pizzetti A, Puccetti S, Ricci C, Tombesi F, Torres-Albà N and Wong K-W (2024), The high energy X-ray probe (HEX-P): constraining supermassive black hole growth with population spin measurements.
Front. Astron. Space Sci. 11:1324796.
doi: 10.3389/fspas.2024.1324796

The high energy X-ray probe (HEX-P): constraining supermassive black hole growth with population spin measurements

J. M. Piotrowska[1]*, J. A. García[1,2], D. J. Walton[3], R. S. Beckmann[4], D. Stern[5], D. R. Ballantyne[6], D. R. Wilkins[7], S. Bianchi[8], P. G. Boorman[1], J. Buchner[9], C.-T. Chen[10,11], P. Coppi[12], T. Dauser[13], A. C. Fabian[4], E. Kammoun[8,14,15], K. Madsen[2], L. Mallick[1,16,17]†, G. Matt[8], G. Matzeu[18], E. Nardini[15], A. Pizzetti[19], S. Puccetti[20], C. Ricci[21,22], F. Tombesi[2,23,24,25,26], N. Torres-Albà[19] and K.-W. Wong[27], on behalf of the HEX-P Collaboration

[1]Cahill Center for Astronomy and Astrophysics, California Institute of Technology, Pasadena, CA, United States, [2]X-ray Astrophysics Laboratory, NASA Goddard Space Flight Center, Greenbelt, MD, United States, [3]Centre for Astrophysics Research, University of Hertfordshire, Hatfield, United Kingdom, [4]Institute of Astronomy, University of Cambridge, Cambridge, United Kingdom, [5]Jet Propulsion Laboratory, California Institute of Technology, Pasadena, CA, United States, [6]Center for Relativistic Astrophysics, School of Physics, Georgia Institute of Technology, Atlanta, GA, United States, [7]Kavli Institute for Particle Astrophysics and Cosmology, Stanford University, Stanford, CA, United States, [8]Dipartimento di Matematica e Fisica, Università Roma Tre, Rome, Italy, [9]Max-Planck-Institut für Extraterrestrische Physik (MPE), Garching, Germany, [10]Marshall Space Flight Center, Huntsville, AL, United States, [11]Science and Technology Institute, Universities Space Research Association, Huntsville, AL, United States, [12]Department of Astronomy, Yale University, New Haven, CT, United States, [13]Dr Karl Remeis-Observatory and Erlangen Centre for Astroparticle Physics, FAU Erlangen-Nürnberg, Bamberg, Germany, [14]UMR5277 Institut de Recherche en Astrophysique et Planétologie (IRAP), Toulouse, France, [15]INAF–Osservatorio Astrofisico di Arcetri, Firenze, Italy, [16]University of Manitoba, Department of Physics and Astronomy, Winnipeg, MB, Canada, [17]Canadian Institute for Theoretical Astrophysics, University of Toronto, Toronto, ON, Canada, [18]Quasar Science Resources SL for ESA, European Space Astronomy Centre, Science Operations Department, Madrid, Spain, [19]Department of Physics and Astronomy, Clemson University, Kinard Lab of Physics, Clemson, SC, United States, [20]ASI–Agenzia Spaziale Italiana, Rome, Italy, [21]Instituto de Estudios Astrofísicos, Facultad de Ingeniería y Ciencias, Universidad Diego Portales, Santiago, Chile, [22]Kavli Institute for Astronomy and Astrophysics, Peking University, Beijing, China, [23]Physics Department, Tor Vergata University of Rome, Rome, Italy, [24]INAF–Astronomical Observatory of Rome, Rome, Italy, [25]INFN–Rome Tor Vergata, Rome, Italy, [26]Department of Astronomy, University of Maryland, College Park, MD, United States, [27]Department of Physics, SUNY Brockport, Brockport, NY, United States

Constraining the primary growth channel of supermassive black holes (SMBHs) remains one the most actively debated questions in the context of cosmological structure formation. Owing to the expected connection between SMBH spin parameter evolution and the accretion and merger history of individual black holes, population spin measurements offer a rare observational window into the cosmic growth of SMBHs. As of today, the most common method for estimating SMBH spin relies on modeling the relativistically broaden atomic profiles in the reflection spectrum observed in X-rays. In this paper, we study the observational requirements needed to confidently distinguish between the primary SMBH growth channels based on their distinct spin-mass distributions predicted by the

Horizon-AGN cosmological simulation. Indoing so, we characterize outstanding limitations associated with the existing measurements and discuss the landscape of future observational campaigns which could be planned and executed with future X-ray observatories. We focus our attention on the *High-Energy X-ray Probe (HEX-P)*, a proposed probe-class mission designed to serve the high-energy community in the 2030s.

KEYWORDS

supermassive black holes, AGN, black hole growth, black hole spin, future X-ray observatories

1 Introduction

As of today, the existence of supermassive black holes (SMBHs) residing in the nuclei of galaxies is no longer a subject of scientific dispute. With the presence of an SMBH clearly revealed in the orbital motion of stars in our Galactic center (e.g., Ghez et al., 2008; Genzel et al., 2010) and direct imaging of matter just outside the Event Horizon (Event Horizon Telescope Collaboration et al., 2019; Event Horizon Telescope Collaboration et al., 2022), the focus has now shifted towards understanding the origin and growth of these extreme astrophysical objects with masses above $\gtrsim 10^6 \mathrm{M}_\odot$. Decades of extragalactic observations have demonstrated a tight connection between the properties of SMBHs and their galactic hosts, now interpreted as black hole-galaxy co-evolution across cosmic time (see Kormendy and Ho, 2013, for a review). More specifically, SMBHs have been established as key players in shaping galaxy formation, structure and, most of all, in suppressing galactic star formation through a range of highly energetic processes collectively referred to as active galactic nucleus (AGN) feedback (e.g., McNamara et al., 2000; Bower et al., 2006; Terrazas et al., 2016; Henriques et al., 2019; Piotrowska et al., 2022).

Regardless of its exact mode of operation, AGN feedback relies on extracting power from the immediate surroundings of supermassive black holes via accretion. The amount of energy released in the process greatly exceeds the threshold required to offset cooling around galaxies or to unbind baryons within them, rendering SMBHs a formidable source of power capable of affecting their galactic hosts (see Fabian, 2012; Werner et al., 2019, for in-depth reviews). At high accretion rates ($\dot{M}_{\mathrm{BH}} \gtrsim 0.01\dot{M}_{\mathrm{Edd}}$, the Eddington accretion rate[1]), matter surrounding an SMBH is thought to infall through a geometrically thin, optically thick accretion disk (Novikov and Thorne, 1973; Shakura and Sunyaev, 1973) in which emitted radiation drives high-velocity *quasar* outflows (e.g., Murray et al., 1995; King et al., 2008; Faucher-Giguère and Quataert, 2012) coupling to the interstellar medium (ISM) and further accelerating it at galaxy-wide scales (e.g., Feruglio et al., 2010; Hopkins and Quataert, 2010; Villar-Martín et al., 2011; Maiolino et al., 2012; Cicone et al., 2014; Fiore et al., 2017). At low accretion rates $\lesssim 10^{-6}\ \dot{M}_{\mathrm{Edd}}$, the inflow forms a geometrically thick, optically thin accretion disk (e.g., Yuan and Narayan, 2014; Giustini and Proga, 2019) and launches *relativistic jets* which deposit energy within the circumgalactic medium (CGM) at large distances away from the galactic host (e.g., McNamara et al., 2000; Bîrzan et al., 2004; Hlavacek-Larrondo et al., 2012; 2015; Werner et al., 2019). Across all flavors of AGN feedback processes, the efficiency with which power is extracted from the accretion flow depends on the angular momentum of the SMBH and spans over an order of magnitude in range (e.g., Thorne, 1974; Penna et al., 2010; Avara et al., 2016; Liska et al., 2019), further broadening the range of impact AGN can have on their host galaxies.

Although abundant observational evidence exists for the impact of SMBHs on their surrounding galaxies, relatively little is known about their origins and growth across cosmic time. Understanding how these black holes form and reach their impressive masses is particularly important both in the context of galaxy evolution and recent *James Webb Space Telescope* (*JWST*, Gardner et al., 2023; Rigby et al., 2023) observations, which report black holes with masses $M_{\mathrm{BH}} > 10^6 \mathrm{M}_\odot$ as early as $z = 10.6$ (Harikane et al., 2023; Maiolino et al., 2023a; Maiolino et al., 2023b). Since cosmic growth via accretion of gas and SMBH-SMBH mergers occurs on timescales beyond direct human observation, one would, ideally, like to characterize SMBH growth histories using alternative observables. An example of such a proxy is black hole angular momentum, $\vec{J}$, which changes its orientation and magnitude in response to the different physical processes that increase M_{BH}. Hence, by *measuring the magnitude of SMBH angular momentum J,* usually expressed in terms of the dimensionless spin parameter ($a^* \equiv Jc/GM_{\mathrm{BH}}^2$, where c is the speed of light and G is the gravitational constant), *one can extract information about the past record of its growth.* In AGN, spin parameter can be estimated by modelling coronal X-ray radiation reprocessed (or "reflected") by the accretion disk (e.g., Fabian et al., 1989; Laor, 1991). Because the reflected signal depends on the position of the innermost edge of the accretion disk, this relationship can be directly applied to determine $a*$ in nearby SMBHs (see Section 3.2 for an overview of this approach).

As the black hole increases its mass via accretion of surrounding material, its spin changes owing to angular momentum transfer from the accretion flow. If the accreting material settles into a prograde[2] disk, inflow of angular momentum aligned with that of the black hole leads to its efficient spin-up (Bardeen, 1970; Moderski and

---

[1] Accretion rate associated with Eddington luminosity, L_{Edd} at which outward radiation pressure balances the gravitational force outside a massive body with mass M, given by $L_{\mathrm{Edd}} = 4\pi GMc/\kappa$, where κ is the opacity of the accreting material, G the gravitational constant and c the speed of light.

[2] In a prograde disk, the accreting material and the black hole are both rotating in the same direction.

Sikora, 1996; Moderski et al., 1998). In contrast, chaotic accretion of matter with randomly oriented angular momentum decreases the spin magnitude, ultimately driving it towards $a* \sim 0$ over sufficiently long times (e.g., Berti and Volonteri, 2008; King et al., 2008; Dotti et al., 2013). In the presence of magnetic fields, even in the case of ordered inflow through aligned accretion disks, spin can also be reduced by energy extraction via the Blandford-Znajek process (Blandford and Znajek, 1977). This jet launching mechanism has been shown to drain black hole angular momentum in magnetically arrested disks (MADs) in General-Relativistic magneto-hydrodynamical (GRMHD) simulations of SMBH accretion (e.g., Tchekhovskoy et al., 2011; McKinney et al., 2012; Tchekhovskoy et al., 2012; Narayan et al., 2022; Curd and Narayan, 2023; Lowell et al., 2023). Finally, mergers of SMBH binaries leave behind remnants which can be either spun up or down with respect to their progenitors, contingent on individual spin parameters upon coalescence (e.g., Kesden, 2008; Rezzolla et al., 2008; Tichy and Marronetti, 2008; Barausse and Rezzolla, 2009; Healy et al., 2014; Hofmann et al., 2016).

Depending on the relative contribution of these processes across cosmic time, one would expect different growth histories of SMBHs to leave an imprint on the measured spin parameter. In the cosmological context, this expectation was first explored in semi-analytic models (SAMs) - taking advantage of their low computational cost, several studies have now used SAMs to make spin population predictions for different SMBH accretion and coalescence scenarios. Berti and Volonteri (2008) demonstrated that prolonged episodes of coherent accretion produce SMBH populations spinning at near-maximal rates, while chaotic infall of matter and mergers force the dimensionless spin parameter towards $a* \sim 0$. Dotti et al. (2013) generalized the chaotic accretion paradigm and found that SMBHs are not spun down efficiently when the distribution of accreted angular momenta is not isotropic, allowing black holes to maintain stable high spin values for even modest degrees of anisotropy. By linking the orientation of accreted angular momentum with that of the galactic host, Sesana et al. (2014) further showed that the spin parameter critically depends on the dynamics of the host and that SMBHs residing in spiral galaxies tend to spin fast, biasing the observable samples towards high $a*$ values.

Moving beyond the idealized semi-analytic approach, spin parameter modelling in hydrodynamical cosmological simulations only recently became an area of active development (Dubois et al., 2014c; Fiacconi et al., 2018; Bustamante and Springel, 2019; Talbot et al., 2021; Talbot et al., 2022). As of today, there exist three major simulation suites which trace spin parameter in statistical samples of SMBHs: the *NewHorizon cosmological simulation* (Dubois et al., 2021), on-the-fly[3] spin evolution coupled to AGN feedback prescription in a $(16Mpc)^3$ volume, simulated down to $z = 0.25$ at a maximum spatial resolution of 34 pc; the Bustamante and Springel (2019) *simulation suite*, on-the-fly spin evolution implemented in the moving-mesh code AREPO (Springel, 2010), with a cosmological volume of $(\sim 37Mpc)^3$ and a spatial resolution of ~1 kpc, which is evolved to $z = 0$ with the IllustrisTNG AGN feedback model (Weinberger et al., 2017); and the *Horizon-AGN cosmological simulation* (Dubois et al., 2014b), in which spin evolution is computed via post-processing of the completed Horizon-AGN run Dubois et al., 2014a, followed down to $z = 0$ in a $(\sim 147Mpc)^3$ volume at maximum spatial resolution of $\sim 1kpc$. All three suites produce realistic populations of SMBHs and yield $a*$ population statistics compatible with those observed in the local Universe. With limited sample sizes and generous uncertainty on individual measurements, currently available observations are not constraining enough to indicate preference for any particular model. In the future, increased measurement precision and improved statistics in the $M_{\rm BH} - a*$ plane will be of critical importance for new generations of spin evolution models: with improved calibration targets for subgrid prescriptions, different hydrodynamical cosmological models are likely to further converge over time, allowing us to use $a*$ constraints as an interpretative tool, as opposed to a means of discriminating among modelling approaches.

In this study, we show how future observing programs targeting statistical samples of SMBH spins and masses can be designed to best discriminate between different growth histories of SMBHs. We choose to focus on the Horizon-AGN cosmological simulation to take advantage of its SMBH statistics delivered over a large simulation volume. Treating the simulation suite as a case study, we determine sample sizes and measurement precisions required to differentiate between accretion- and merger-dominated SMBH growth. We then discuss these requirements in the context of the *High-Energy X-ray Probe* (*HEX-P*; Madsen et al. 2023)–a probe-class mission concept which offers sensitive broad-band X-ray coverage (0.2–80 keV) with exceptional spectral, timing and angular capabilities, featuring a High Energy Telescope (HET) that focuses hard X-rays, and a low energy telescope (LET) that focuses low-energy X-rays. Taking into account the *HEX-P* instrument design, we demonstrate the potential for this mission to deliver SMBH spin parameter measurements sufficient to constrain SMBH growth scenarios.

In Section 2 we discuss the challenges associated with spin modelling in cosmological hydrodynamical simulations and briefly describe the Horizon-AGN suite. Section 3 provides an overview of reflection spectroscopy as a tool for measuring $a*$, followed by a discussion on current constraints and their comparison with the Horizon-AGN cosmological model in Section 4. Section 5 motivates a systematic study of the $M_{\rm BH} - a*$ plane with future observing programs, and Section 6 describes a sample of AGN selected from the BAT AGN Spectroscopic Survey appropriate for such a study. In Section 7 we determine minimum sample requirements for differentiating between accretion- and merger-dominated SMBH growth, followed by *HEX-P* spin parameter recovery simulations in Section 8. In Section 9 we demonstrate the potential for *HEX-P* to characterize SMBH growth histories through population spin measurements and present our final remarks in Section 10.

2 SMBH spin in cosmological hydrodynamical simulations

Tracing the change in SMBH spin in the context of large-scale evolution of the Universe is a complex problem spanning a broad range of spatial and temporal scales. Transfer of angular momentum via accretion in disks occurs on size scales between ~1 and a

---

[3] The term *on-the-fly* refers to a spin calculation explicitly included at runtime within the simulation, as opposed to in post-processing after the simulation run is completed.

few 10^2 gravitational radii $R_G = GM_{\mathrm{BH}}/c^2$ (e.g., Fausnaugh et al., 2016; Jiang et al., 2017; Cackett et al., 2018; Edelson et al., 2019; Guo et al., 2022; Homayouni et al., 2022), which then couples to gas inflows from the host galaxy on scales of several hundred pc (e.g., García-Burillo et al., 2005; Hopkins and Quataert, 2010; Wong et al., 2011; Wong et al., 2014; Alexander and Hickox, 2012; Russell et al., 2015; Russell et al., 2018), ultimately fuelled by gas accretion from within the cosmic web on the intergalactic scales of hundreds of kpc (e.g., Sancisi et al., 2008; Putman et al., 2012; Tumlinson et al., 2017). At the same time, gas flows at all scales are affected by the non-trivial interplay of feedback processes from both stars (e.g., Katz et al., 1996; Cole et al., 2000; Kereš et al., 2005; Hopkins et al., 2014) and AGN (e.g., Bower et al., 2006; Croton et al., 2006; Fabian, 2012; Kormendy and Ho, 2013), disk instabilities (e.g., Schwarz, 1981; Athanassoula et al., 1983; Kuijken and Merrifield, 1995; Debattista et al., 2006) and galaxy-galaxy interactions (e.g., Toomre and Toomre, 1972; Sanders et al., 1988; Barnes and Hernquist, 1992; Di Matteo et al., 2005; Springel et al., 2005; Hopkins et al., 2006) all of which, ideally, need to be taken into account in a comprehensive modelling of SMBH spin evolution. The dynamic range in size scales alone renders it computationally unfeasible to directly follow SMBH evolution, even with current state-of-the-art hardware and numerical methods (see Vogelsberger et al., 2020; Crain and van de Voort, 2023, for reviews of the current state of the field). Hence, to overcome these limitations, cosmological simulations replace missing baryonic physics with *subgrid*[4] prescriptions—semi-analytic models relying on astrophysical scaling relations to predict large scale hydrodynamic effects of unresolved AGN accretion, spin evolution and feedback.

There currently exist three cosmological hydrodynamical simulations which either model spin on-the-fly (Bustamante and Springel, 2019; Dubois et al., 2021) or calculate its evolution in post-processing (Dubois et al., 2014b) (see Section 1). Although these three studies differ significantly in their subgrid prescriptions, in addition to spanning different cosmological volumes and final simulation redshifts, they all deliver SMBH spin distributions broadly consistent with the currently available observational constraints. As spin modelling in a full cosmological context is still in its infancy, the agreement between both models themselves and with the observable Universe is likely to improve once better constraints are available for subgrid parameter tuning. Thus, the study presented here does not focus on differentiating among currently available models, but rather on demonstrating the capability of *HEX-P* to identify different SMBH growth channels within a single realization of a sophisticated full-physics model of the Universe.

2.1 Horizon-AGN cosmological model

In our study we make use of the Horizon-AGN cosmological simulation (Dubois et al., 2014a), post-processed to trace SMBH spin evolution in response to local hydrodynamics of gas, accretion and SMBH mergers (Dubois et al., 2014b). Our choice of the simulation suite is motivated by its large volume of $(\sim 100\mathrm{cMpc})^3$, generous statistics and great success in reproducing realistic SMBH and galaxy samples across cosmic time (Dubois et al., 2016; Volonteri et al., 2016; Beckmann et al., 2017; Kaviraj et al., 2017). Most importantly, however, accretion-dominated and accretion + merger growth histories of SMBHs in Horizon-AGN have been shown to result in distinct spin parameter distributions (Beckmann et al., 2023), hence the suite offers a promising opportunity for studying the SMBH growth signal with *HEX-P* reflection spectroscopy. The full Horizon-AGN suite, including its spin parameter evolution model, are described in detail in Dubois et al. (2014a) and Dubois et al. (2014b); here we only provide a brief overview of SMBH treatment in the simulation.

Horizon-AGN is a suite of cosmological, hydrodynamical simulations performed with the RAMSES code (Teyssier, 2002) for ΛCDM cosmology with cosmological parameter values based on WMAP-7 observations ($H_0 = 70.4\mathrm{kms}^{-1}Mpc^{-1}$, $\Omega_m = 0.272$, $\Omega_b = 0.045$, $\Omega_\Lambda = 0.728$ and $\sigma_8 = 0.81$; Komatsu et al., 2011). The hydrodynamics are computed on an adaptively refined Cartesian grid coupled to subgrid prescriptions for baryonic interactions, including gas cooling, star formation, black hole accretion and feedback processes described in detail in Dubois et al. (2014a). The simulation only includes black holes of the supermassive kind, seeding them in $z > 1.5$ gas cells once these exceed a star formation threshold of $n_0 = 0.1\mathrm{H}cm^{-1}$ in density. Once seeded, the SMBHs then accrete via a boosted Bondi-Hoyle-Lyttleton prescription ($\dot{M}_{\mathrm{BH}} = 4\pi\alpha G^2 M_{\mathrm{BH}}^2 \bar{\rho}/(\bar{c}_s^2 + \bar{u}^2)^{3/2}$, where $\bar{u}$, $\bar{\rho}$ and $\bar{c}_s$ are gas velocity, density and speed of sound averaged in the SMBH vicinity, and G is the gravitational constant; Hoyle and Lyttleton, 1939; Bondi and Hoyle, 1944; Bondi, 1952) capped at the Eddington rate. A fraction $\epsilon_r = 0.1$ of the accreted rest-mass energy is then released as AGN feedback with $\dot{E}_{\mathrm{AGN}} = \epsilon_r \dot{M}_{\mathrm{BH}} c^2$, and the fraction of power coupled to gas is controlled by the accretion rate-dependent feedback mode. For Eddington ratios $f_{\mathrm{Edd}} \equiv \dot{M}_{\mathrm{BH}}/\dot{M}_{\mathrm{Edd}} > 0.01$, the AGN is in the “quasar” mode and isotropically injects 0.15 $\dot{E}_{\mathrm{BH}}$ as thermal energy around the SMBH particle. For $f_{\mathrm{Edd}} < 0.01$ the AGN switches to “radio” mode feedback, releasing all $\dot{E}_{\mathrm{BH}}$ in biconical outflows. In a post-processing procedure introduced in Dubois et al. (2014b), SMBH are assumed to begin with a spin of $a* = 0$, which subsequently evolves in response to accretion of gas from the hydrodynamical grid and SMBH-SMBH mergers across cosmic time. The spin evolution model combines semi-analytic considerations and calibrations extracted from GRMHD simulations to model the two phenomena, including spin evolution in misaligned disks via the Bardeen-Peterson effect. The prescription, however, does not model SMBH spin-down due to jets via the Blandford-Znajek mechanism.

3 Observations of black holes

Astrophysical black holes are unique objects of great interest as they represent the ultimate test of General Relativity as a theory for gravity. Despite their exotic phenomenology, black holes are also objects of outstanding simplicity; owing to the no-hair theorem (Israel, 1967; Israel, 1968; Carter, 1971), they are fully described by only three physical quantities: mass, angular momentum (or spin),

---

[4] Capturing physics at scales smaller than those allowed by numerical resolution via semi-analytic prescriptions coupled to quantities directly resolved in the simulation. See Vogelsberger et al. (2020) and Crain and van de Voort (2023) for comprehensive reviews of the methodology.

and electric charge. Furthermore, charge is quickly neutralized in any realistic astrophysical environment (Michel, 1972; Wald, 1984; Novikov and Frolov, 1989; Treves and Turolla, 1999; Bambi, 2017), leaving just mass and spin as the fundamental parameters to be constrained by observations.

3.1 Mass

Of the two properties describing a black hole, mass is likely the most straightforward to measure (both for stellar mass black holes and SMBHs). Indeed, a range of techniques has now been developed for SMBH mass estimation, appropriate for both local and distant sources. For a relatively nearby system (such as the SMBH in the center of our Galaxy), it is possible to resolve the motion of individual stars and model the underlying gravitational potential to estimate its associated black hole mass (e.g., Ghez et al., 1998; Ghez et al., 2008; Genzel et al., 2010; Gravity Collaboration et al., 2018). Owing to extremely high resolution requirements, such studies can only be undertaken within the Milky Way, while extragalactic $M_{\rm BH}$ measurements are instead forced to rely on stellar, gas and maser kinematics (e.g., Kormendy et al., 1998; Magorrian et al., 1998; Gebhardt et al., 2000).

One of the most robust methods for measuring $M_{\rm BH}$ for active SMBHs in other galaxies involves reverberation mapping of broad emission lines (Blandford and McKee, 1982; Peterson, 1993). In this approach, the velocity dispersion of gas in the broad line region (BLR) is combined with a measurement of the time delay between variations in the continuum and the line emission to infer the dynamics of the accretion disks (see, e.g., Peterson et al., 2004, for a description of the methodology). The mass estimate relies on the proportionality[5] $M_{\rm BH} \propto R_{\rm BLR}(\Delta V)^2$ between SMBH mass, the line-of-sight velocity of BLR gas (ΔV, encoded in emission line profiles) and the distance between the black hole and the BLR ($R_{\rm BLR}$, inferred from the time lag measurement). Since observations of this kind require monitoring over long times at prime facilities, the current sample of SMBH masses measured via reverberation contains only ~100 objects in total (e.g., Woo et al., 2015).

Because of the limited number of direct SMBH mass measurements, statistical studies commonly rely on empirical calibrations to estimate $M_{\rm BH}$. A common alternative to the expensive reverberation mapping observations combines continuum luminosity measurements and BLR emission line width to estimate $M_{\rm BH}$. Known as the “single-epoch virial BH mass estimator”, the method relies on a tight relation between continuum (or line) luminosity and $R_{\rm BLR}$ observed among the reverberation mapping targets, providing a calibrated estimator without the need for a time-lag measurement in each source (see Shen, 2013, for an in-depth review of the method and its limitations). Owing to a broad similarity in continuum and emission line strength among quasars, this method has been successfully applied in estimating $M_{\rm BH}$ in various quasar samples at both low and high redshift, using observations in X-ray, rest-frame UV and optical wavelengths (e.g., Vestergaard, 2002; Greene and Ho, 2005; Wang et al., 2009; Trakhtenbrot and Netzer, 2012).

Absent necessary nuclear emission lines, another common flavor of empirical calibrations makes use of the measured properties of SMBH galactic hosts to estimate their mass. Among these, the relationship between stellar velocity dispersion in the galactic bulge and SMBH mass measured via reverberation mapping, the $M_{\rm BH} - \sigma *$ relation, boasts the least scatter, yielding a systematic uncertainty of ~$0.3 - 0.5$ dex in $\log(M_{\rm BH})$ (Ferrarese and Merritt, 2000; Hopkins et al., 2011; McConnell and Ma, 2013; Saglia et al., 2016). Although subject to significant scatter at present, these calibrations will improve with the arrival of future large multi-epoch observation programs like the Black Hole Mapper (Kollmeier et al., 2019). The planned ~1000 optical reverberation mapping $M_{\rm BH}$ estimates will significantly increase the robustness and precision of the $M_{\rm BH} - \sigma *$ estimation. Other techniques have also been recently proposed to measure $M_{\rm BH}$ using X-ray variability, such as X-ray reverberation (Alston et al., 2020) and X-ray spectral-timing (Ponti et al., 2012; Ingram et al., 2022), both of which can be model dependent and carry systematic uncertainties that still need to be understood.

3.2 Spin

The estimation of black hole spin, on the other hand, is a more difficult task as it mainly impacts the environment extremely close to the black hole. For example, the black hole’s angular momentum determines the radius of the innermost stable circular orbit, ISCO ($R_{\rm ISCO}$, which varies from 9 $R_{\rm G}$ for a maximal retrograde spin to ~1.2 $R_{\rm G}$ for a maximal prograde spin of $a* = 0.998$, where $R_{\rm G} = GM_{\rm BH}/c^2$ is the gravitational radius; Bardeen et al., 1972; Thorne, 1974). In principle, the spin of a black hole can be constrained through a variety of methods, most of which involve determining $R_{\rm ISCO}$, but for AGN the most reliable method currently available comes via characterization of relativistic reflection from the innermost accretion disk (sometimes referred to as the iron-line method; see Reynolds 2021for a recent review).

For moderately high accretion rates, most of the infalling material is expected to flow through a thin, optically-thick accretion disk (Shakura and Sunyaev, 1973). Some of the thermal emission from the disk, which peaks in the UV for most AGN, is Compton up-scattered into a much higher energy continuum by a “corona” of hot electrons ($kT_{\rm e} \sim 100$ keV; Fabian et al., 2015; Baloković et al., 2020), which is the primary source of X-ray emission in AGN[6]. This X-ray emission re-irradiates the surface of the disk, producing a further “reflected” emission component that contains a diverse range of atomic spectral features both in emission and absorption. Among these, the inner-shell transitions from Fe ions—predominantly the Kα emission line at 6.4–6.97 keV (depending on the ionization state)—together with a strong absorption K-edge around 7–8 keV, are typically the most prominent. Additionally, reflection spectra exhibit a characteristic high-energy continuum, peaking at ~30 keV, often referred to as the “Compton hump” (George and Fabian,

---

[5] The proportionality constant, known as the virial factor, is challenging to determine for individual objects owing to the unknown geometry of the BLR gas (e.g., Brewer et al., 2011; Pancoast et al., 2014).

[6] The precise nature of the corona is still poorly understood, but is also an area of AGN physics that *HEX-P* will help uncover (Kammoun et al. 2023).

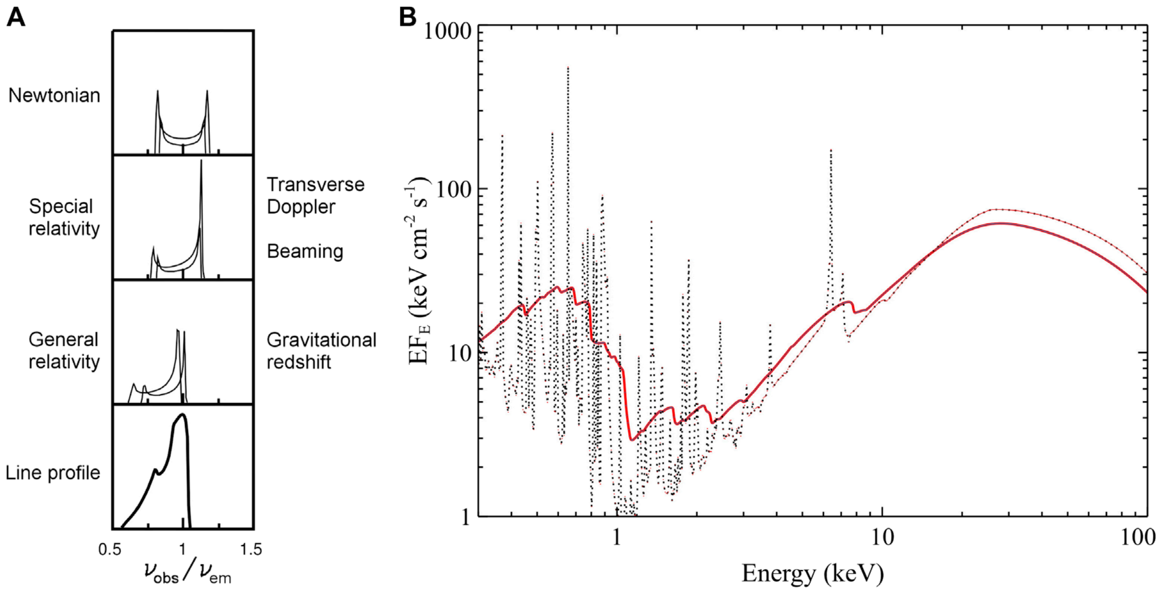

FIGURE 1
(A)*:* The broadening experienced by a narrow emission line from an accretion disk around a black hole (from Fabian et al., 2000). The top three panels show the effects of Newtonian gravity, Special Relativity and General Relativity, respectively, on the line profiles for two example radii within the disk, while the bottom panel shows the broadened and skewed "diskline" profile expected when these combined effects are integrated over the full radial profile of the disk. **(B)***:* An example of these relativistic effects applied to a typical reflection spectrum from moderately ionized material (as may be expected for the accretion disk in an AGN). Here we use the XILLVER reflection model for the rest-frame reflection spectrum (dotted line; García and Kallman, 2010) and apply the relativistic blurring with the RELCONV model (solid line; Dauser et al., 2010).

1991; Ross and Fabian, 2005; García and Kallman, 2010). Although the emission lines are narrow in the frame of the disk, by the time the material in the disk approaches the ISCO it is orbiting at relativistic speeds, and the gravitational redshift is also very strong. The combination of these effects serves to broaden and skew the emission lines from our perspective as a distant, external observer, resulting in a characteristic "diskline" emission profile (Fabian et al., 1989; Laor, 1991; Brenneman and Reynolds, 2006; Dauser et al., 2010; see Figure 1). Provided that the disk extends all the way into the ISCO orbit, also expected at moderately high accretion rates, then characterizing the relativistic blurring gives a measurement of R_{ISCO}, and thus of $a*$. These distortions are most often discussed in the context of the iron emission line specifically, as it is typically the strongest spectroscopically isolated emission line in the reflection spectrum. While the iron emission provides the cleanest view of the broadened line profile, these relativistic effects impact the whole reflection spectrum (see Figure 1).

This approach to measuring spin is particularly powerful as it can be applied to black holes of all masses, not just the SMBHs powering AGN (e.g., Walton et al., 2012). Indeed, relativistically broadened Fe K lines have been observed in the spectra of a large fraction of AGN with high signal-to-noise (S/N) X-ray spectra (e.g., Tanaka et al., 1995; Miniutti et al., 2007; Fabian et al., 2009; de La Calle Pérez et al., 2010; Brenneman et al., 2011; Gallo et al., 2011; Nardini et al., 2011; Parker et al., 2014; Ricci et al., 2014; Wilkins et al., 2015; Jiang et al., 2018; Walton et al., 2019) as well as most well-studied black hole X-ray binaries (e.g., Miniutti et al., 2004; Miller et al., 2009; Reis et al., 2009; Duro et al., 2011; King et al., 2014; García et al., 2015; Walton et al., 2017; Xu et al., 2018; Kara et al., 2019; Tao et al., 2019; Jiang et al., 2022; Draghis et al., 2023; see also Connors et al. (2023) for additional discussion of black hole X-ray binary studies with *HEX-P*). Broadband X-ray spectroscopy is particularly critical for properly characterizing the reflected emission: its key features span the entire observable X-ray band (a diverse set of emission lines from lighter elements at energies $\lesssim 2keV$, the iron emission line at ~6–7 keV and the Compton hump at ~30 keV) and their proper modelling requires an accurate characterization of the continuum across the entire broadband range. The *NuSTAR* era has therefore marked a period of exciting progress in this field, finally providing high S/N spectroscopy up to ~80 keV for AGN. *NuSTAR* observations have unambiguously revealed the high-energy reflected continuum associated with the broad iron emission, and have been particularly powerful when paired with simultaneous lower-energy coverage from, e.g., *XMM-Newton*, confirming our ability to measure spin via reflection spectroscopy (e.g., Risaliti et al., 2013; Marinucci et al., 2014; Walton et al., 2014; Buisson et al., 2018; García et al., 2019; Chamani et al., 2020; Wilkins et al., 2022). As we further show in Section 4, however, these currently available samples are still insufficient to characterize modelled SMBH growth histories in the observable Universe.

4 Current constraints: The spin–mass plane

The most recent systematic compilations of SMBH spins and masses from the literature are presented in Reynolds (2021) and Bambi et al. (2021). In addition, there have been a few more measurements made since the publication of these reviews

(Walton et al., 2021; Mallick et al., 2022; Sisk-Reynés et al., 2022), resulting in a current sample size of 46 SMBHs with at least initial spin constraints. All but three of these sources are from the local Universe ($z \leq 0.30$, and even then most have $z \leq 0.10$); the two highest redshift constraints to date come from strongly-lensed quasars ($z = 0.66$ and $z = 1.70$; Reis et al., 2014; Reynolds et al., 2014).

Figure 2 shows the current constraints in the spin-mass plane for SMBHs with masses above $10^6 M_\odot$, compared against two distinct SMBH populations in the Horizon-AGN cosmological simulation. Grey filled diamonds indicate measurements with 1σ error bars[7], while open diamonds mark lower limits on $a*$. Many of the measurements show evidence for rapidly rotating black holes, particularly for masses in the range $M_{\rm BH} \sim 10^6$–$10^7 M_\odot$. There are hints in the current data of trends towards lower spins, or at least an increase in the spread of spin measurements, at higher masses, particularly for $M_{\rm BH} > 10^8 M_\odot$.

In order to better capture these trends, we further calculate mean spin parameter values in three bins of SMBH mass between 10^6 and $10^{10} M_\odot$[8], marked with open black squares. In the mean calculation we treat all available constraints as uncensored measurements and hence arrive at lower limit estimates in each bin, which indicate a tentative decrease in $a*$ with increasing $M_{\rm BH}$. We note, however, that there are still only a few measurements in the high-mass regime, and the uncertainties on those are also large. Furthermore, although a few sample-based efforts to constrain SMBH spin via systematic relativistic reflection analyses exist (e.g., Walton et al., 2013; Mallick et al., 2022), the majority of these measurements come from independent analyses of individual sources. As such, they are heterogeneous in regard to the reflection and relativistic blurring models used, the precise assumptions adopted in the use of these models, and the energy range over which the analysis has been performed. Moreover, *NuSTAR* has only contributed to ~half of these measurements, so not all are based on high S/N broadband X-ray spectroscopy.

The blue and orange shaded regions in Figure 2 indicate regions of the spin-mass parameter plane occupied by different SMBH growth histories in the Horizon-AGN cosmological simulation, described further in Section 4.1. To enable a fair comparison with current measurement constraints, both simulated SMBH populations have been corrected to best account for biases present in the observations. Among these, a potential likely bias towards high $a*$ values resulting from the expected spin-dependence of the radiative efficiency ($\eta(a*)$) in a relativistic thin-disk solution (Novikov and Thorne, 1973) is frequently discussed in the literature as at least part of the reason for the observed prevalence of near-maximal spin values (e.g., Brenneman et al., 2011; Reynolds et al., 2012). Under the simplifying assumption of a uniform distribution of AGN in the local Universe, the probability of observing a given spin value $a*$ scales with $\eta(a*)$ to power $\frac{3}{2}$ for sources with equal accretion rates in flux-limited surveys (see Supplementary Appendix S1 for further details). The superlinear scaling combined with the steep increase of $\eta(a*)$ for $a* > 0.8$ can have profound implications for inferred spin population statistics in observations.

Figure 3 shows the change in radiative efficiency with spin in geometrically thin relativistic disks (left panel) together with the potential impact the $\eta - a*$ bias can have on the observed spin parameter distributions (two panels on the right). Using a uniform distribution of $a* \sim U(0, 0.998)$ and a normal distribution $a* \sim N(0.5, 0.15)$ as examples, the two panels on the right demonstrate how a probability density function (PDF) of the expected measurements is distorted towards high spin values, shifting the expected mean observed spin values towards $a* \approx 0.67$ and $a* \approx 0.54$ for the two respective input distributions. As demonstrated in the figure, the impact of the $\eta - a*$ bias is critically dependent on the underlying true spin parameter distribution. Therefore, the strength of this effect will differ from our test cases for realistic samples of AGN observations.

Finally, we also note that radiative efficiency estimation for individual sources is challenging in practice. In the case of SMBH populations, however, one can obtain meaningful constraints on typical $\eta(a*)$ by comparing energy density of AGN radiation with local $M_{\rm BH}$ density (e.g., Soltan, 1982; Fabian and Iwasawa, 1999; Marconi et al., 2004; Raimundo et al., 2012). Most recent studies indicate $\eta(a*) \sim 0.12$–0.20, hence favoring spinning SMBH populations and implying $\boldsymbol{a* \gtrsim 0.5}$ (Shankar et al., 2020).

4.1 Connecting to SMBH growth histories in Horizon-AGN

As discussed in Section 2, different modes of SMBH growth leave distinct imprints on their angular momenta. Hence, once integrated over the lifetime of individual black holes, different SMBH growth histories, e.g., accretion-vs. merger-dominated scenarios, yield distinguishable distributions of their spin parameter $a*$. Beckmann et al. (2023) (hereafter B23) study such signatures in the $z = 0.0556$ snapshot of the Horizon-AGN cosmological simulation, finding that black holes grown exclusively via accretion (nearly merger-free) have a spin distribution that is distinct from the rest of the black hole population at $>5\sigma$ significance. As shown in Figure 3 of B23, SMBHs which acquired <10% of their mass in mergers have a significantly narrower distribution of spin parameter values than the remainder of the black hole population, concentrated at spin values close to $a* = 0.998$. The striking contrast between $a*$ populations presents a promising prospect for extending the study into two dimensions—distinguishing SMBH growth histories with measurements in the $M_{\rm BH} - a*$ plane.

To extract predictions for the observable signatures of different SMBH growth histories in the spin-mass plane from Horizon-AGN, we first identify the loci occupied by each history in the $M_{\rm BH} - a*$ parameter space. From here onwards we focus on the $z = 0.0556$ snapshot of the simulation studied in B23, which is well suited for our intended target sample of local AGN (see Section 6.1). Inspired by B23, we use a threshold on $f_{\rm BH,merge}$, the fraction of mass acquired

---

[7] Measurements reported in the literature commonly quote 90% confidence intervals for spin parameter measurements. In order to translate these values to 1σ estimates, we divide the confidence interval by a factor of 1.64, making the simplifying assumption that the current constrains follow split normal distributions.

[8] Our choice of binning scheme is discussed in Section 7.1.

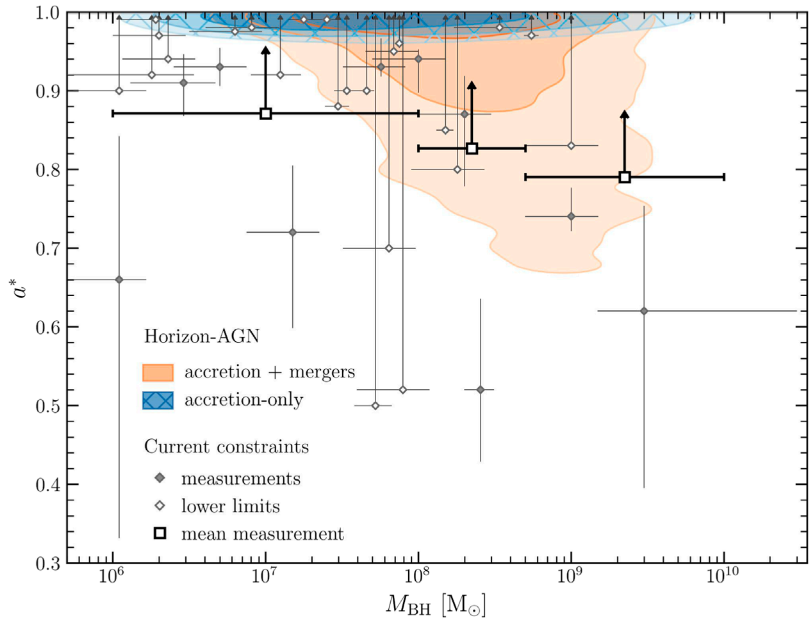

FIGURE 2
Current observational constraints in the $M_{\rm BH} - a*$ plane (open and filled gray diamonds), compared against the locus occupied by the Horizon-AGN cosmological simulation (logarithmically spaced contours) for black holes with $M_{\rm BH} \geq 10^6 M_\odot$ (the range covered by Horizon-AGN). Error bars associated with filled diamonds indicate 1σ uncertainty on $a*$ measurement. Blue, hatched: SMBHs which acquired less than 10% of their mass in mergers (i.e., accretion-only growth), orange: SMBHs with >10% mass grown in mergers (i.e., accretion + mergers growth). Both contours account for the radiative efficiency—spin bias in flux-limited AGN samples. Existing constraints suggest a decreasing trend in $a*$ with $M_{\rm BH}$, as shown by lower limits on mean $a*$ values in $M_{\rm BH}$ bins (black open squares). However, current results are not able to differentiate between SMBH growth scenarios (i.e., orange vs. blue contours).

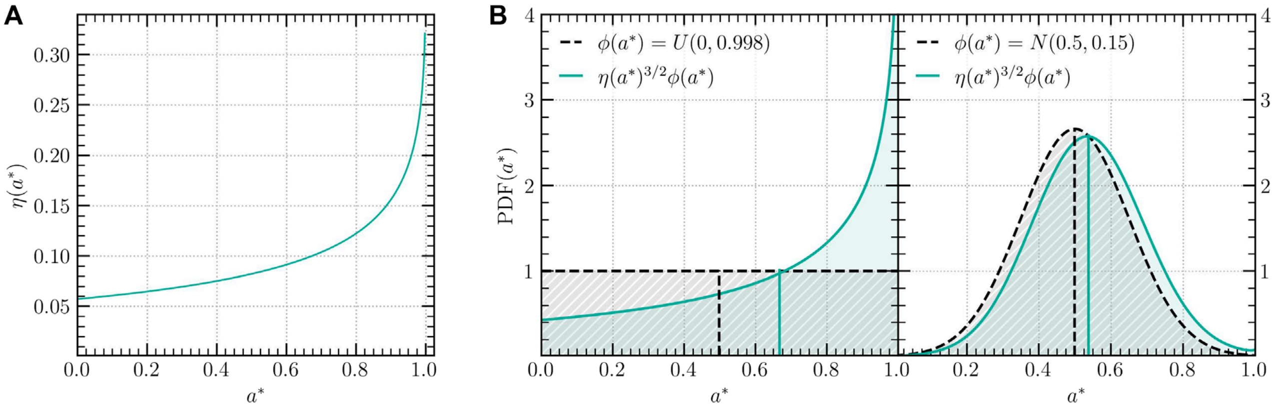

FIGURE 3
(A): Efficiency $\eta(a)$ as a function of spin parameter a for a thin disk solution (Novikov and Thorne, 1973). **(B)**: The effect of spin-dependence of η on the measurement spin population statistics, illustrated with changes to the probability density function (PDF, shaded regions) and its associated mean spin parameter value (vertical lines). Grey hatched regions in the middle and rightmost panels correspond to "raw" PDFs for a uniform distribution $a* \sim U(0, 0.998)$ and a normal distribution centered on $a* = 0.5$ with $\sigma = 0.15$, respectively, while their colored counterparts to PDFs corrected for the $\eta - a*$ bias. The shift between dashed and solid vertical lines indicates the change in associated mean $a*$ value between raw (dashed) and η-bias corrected distributions (solid). The magnitude of bias critically depends on the true underlying spin parameter PDF.

in mergers, to identify the *accretion-only* and *accretion + mergers* growth channels. We adopt $f_{\rm BH,merge} < 0.1$ for accretion-only and $f_{\rm BH,merge} \geq 0.1$ for accretion + mergers, which yield populations of 2,137 and 4,714 black holes respectively. Since the accretion-only population in the simulation is limited to $M_{\rm BH} < 10^{8.5} M_\odot$, to showcase its spin predictions across the entire mass range in Figure 2, we extend the dataset over the missing $M_{\rm BH}$ range with random draws from the accretion-only $a*$ probability density function (PDF). More specifically, we calculate the accretion-only PDF for $M_{\rm BH} > 10^8 M_\odot$ and take random draws from it to generate

$M_{BH} - a*$ value pairs with M_{BH} distribution matching that of the accretion + mergers population above $10^8 M_\odot$. In this way we mimic the effect of switching off spin evolution due to merger events studied for the $z = 0$ snapshot in Dubois et al. (2014b) (see Figure 7 in that publication), arriving at an expected $a*$ measurement across the whole range in M_{BH} for the accretion-only growth channel. We note that although the Eddington-limited subgrid model for SMBH growth in Horizon-AGN does not produce merger-free populations at very high M_{BH}, one could still expect highly spinning black holes at the high-mass end from models which include super-Eddington accretion rates in cosmological hydrodynamical simulations (e.g., Massonneau et al., 2023)[9].

Figure 2 compares loci in the $M_{BH} - a*$ plane occupied by black holes with accretion-only (blue hatched contours) and accretion + mergers (orange filled contours) growth histories in Horizon-AGN. Current observational constraints for $M_{BH} > 10^6 M_\odot$ are shown as individual grey points, with open diamonds corresponding to lower limits and filled diamonds representing measurements and their corresponding 1σ uncertainties. To ensure a meaningful comparison between observations and the cosmological simulation, both of the 2D spin distributions extracted from Horizon-AGN are corrected for the $\eta(a*) - a*$ bias and hence are vertically shifted upwards with respect to the raw output of the simulation. Figure 2 clearly demonstrates that the *two SMBH growth scenarios yield different signatures in the spin–mass parameter space*. At $M_{BH} \gtrsim 10^8 M_\odot$ the two growth histories begin separating, with mergers pushing the expected spin parameter values down towards values as low as $a* \sim 0.6$ with increasing M_{BH}, while the accretion-only scenario remains concentrated at near-maximal spin values. For black hole masses $<10^8$ $M_\odot$ both accretion-only and accretion + mergers populations are concentrated around near-maximal $a*$ values. This degree of overlap is further exacerbated by the spin-dependent radiative efficiency correction, which shifts the orange contours upwards, bringing the two populations towards near-identical loci. Overall, in the context of the Horizon-AGN cosmological simulation, Figure 2 presents a promising opportunity for testing and differentiating between SMBH growth channels in X-ray observations of AGN, even in the presence of the expected $\eta(a*) - a*$ bias.

5 The need for a systematic study of the spin–mass plane

Another critical conclusion drawn from Figure 2 is the necessity of obtaining high-precision spin measurements for large statistical samples of local AGN. Although the current observational constraints are broadly consistent with the accretion + mergers growth channel and show a hint of decrease in $a*$ with M_{BH} above $10^8 M_\odot$, the limited number of measurements at these masses and the relatively poor precision of these measurements mean the current data are not sufficient for a statistical assessment of these trends. More importantly for our discussion, the current sample of 10 measurements and 23 upper limits presented in the figure is not capable of differentiating between the two signatures of SMBH growth histories predicted by Horizon-AGN.

The current state-of-the-art spin measurements also offer a rather limited opportunity for the validation and improvement of the SMBH spin evolution models used in cosmological simulations of SMBH growth. When compared against other hydrodynamical simulations which cover a similar range in M_{BH} (e.g., Bustamante and Springel, 2019), Horizon-AGN produces spin population statistics with only subtle differences in their $M_{BH} - a*$ loci. In general this is encouraging, as it suggests that the qualitative trends implied by these simulations (i.e., Figure 2) are robust. The discrepancies that do exist between them, however, are a combined result of differences in subgrid prescriptions for SMBH seeding, accretion and feedback, and hence carry important information about the validity of a given numerical approach. With the measurement precision and sample size offered by the current constraints, one cannot determine which model implementation (if any) is a closer approximation of the observable Universe. Consequently, the current constraints allow enough room to validate a range of models, while, at the same time, are not strong enough to serve as observational calibrators for future generations of subgrid cosmological SMBH models.

In summary, Figure 2 demonstrates that *a systematic study of the spin-mass plane is necessary for differentiating between different growth histories of SMBHs in the local Universe*. A comprehensive characterisation of M_{BH} and $a*$ properties of local AGN will also play a critical role in calibrating subgrid models of cosmological structure formation by delivering improved constraints on physical properties of SMBH. To establish measurement requirements for these survey observations we take the two SMBH growth histories in Horizon-AGN as a case study, and investigate the precision and sample sizes that would be required to differentiate between these two possibilities in realistic samples of observable sources.

6 The BASS sample

In order to assess the number of known AGN for which spin constraints may be possible, either now or in the moderately near future, we turn to the BAT AGN Spectroscopic Survey (BASS; Koss et al., 2017). This is a major multi-wavelength effort to characterise AGN detected in the very high energy X-ray survey conducted by the Burst Alert Telescope (BAT, 14–195 keV; Barthelmy et al., 2005) onboard the *Neil Gehrels Swift Observatory* (hereafter *Swift*; Gehrels et al., 2004). The latest 105-month release of the BAT source catalogue (Oh et al., 2018) contains 1,632 sources in total, of which 1,105 have been identified as AGN. BASS provides black hole mass estimates (drawn from a variety of methods including Hβ line widths, stellar velocity dispersions and literature searches[10]) and Eddington ratios for the majority of these (e.g., Koss et al., 2022), as well as initial constraints on their broadband spectral properties by combining the BAT data with

---

[9] We also note that efficient SMBH merging is, in part, a consequence of the limitations associated with modelling black hole mergers in cosmological simulations, which do not explicitly follow the SMBH orbital angular momentum loss via dynamical friction.

[10] The method used to estimate the mass for each source is also provided in the BASS catalogue.

the best soft X-ray coverage available (e.g., from *XMM-Newton*; Ricci et al., 2017).

6.1 Sources with spin measurement potential

Not all AGN are well suited to making spin measurements. In particular, the very hard X-ray selection of the BAT survey means it is sensitive to even heavily obscured AGN (including "Compton thick" sources with $N_H > 1.5 \times 10^{24}$ cm^{-2}; e.g., Arévalo et al., 2014; Annuar et al., 2015), and determining the contribution from relativistic reflection becomes increasingly challenging as the source becomes more obscured. Furthermore, there is a general expectation that at low accretion rates the optically-thick accretion disk becomes truncated at radii larger than the ISCO (Narayan and Yi, 1994; Esin et al., 1997; Tomsick et al., 2009), such that the inner radius of the disk no longer provides direct information about the spin. As such, in order to compile a sample of AGN for which spin measurements should be possible, we apply several selection criteria to the BASS sample. First, we select sources with fairly low levels of obscuration, requiring a neutral column density of $N_H \leq 10^{22}$ cm^{-2}. Second, we select sources with Eddington ratios of $\lambda = L_{\mathrm{bol}}/L_{\mathrm{Edd}} \geq 0.01$, so that we may have confidence that the accretion disk should extend to the ISCO (note also that this selection naturally means a black hole mass estimate is available, otherwise it would not have been possible to estimate λ). We further place an upper limit of $\lambda < 0.7$ to select sources for which thin disk approximation is appropriate (e.g., Steiner et al., 2010). We also require that the sources exhibit sufficiently strong reflection features in order for spin measurements to be feasible. We therefore then select sources for which the initial X-ray spectroscopy conducted by Ricci et al. (2017) indicates a reflection fraction consistent with $R \geq 1$ (note that Ricci et al., 2017 use the definition of the reflection fraction from Magdziarz and Zdziarski, 1995). For the same reason, we also exclude blazars from our sample. Finally, after having made these cuts to the BASS data, we also exclude a small number of remaining sources for which the initial X-ray spectroscopy implies an unreasonably hard photon index ($\Gamma \leq 1.5$), taking this as an indication that either the source is actually obscured but that the absorption is sufficiently complex that it was not well characterized by the simple spectral models used in Ricci et al. (2017) or that the spectrum has a low signal-to-noise ratio.

We do not expect these selections to introduce any significant biases that would cause the observed spin distribution to deviate from the intrinsic one (besides the $\eta - a*$ bias that has already been discussed in Section 4). Selecting based on obscuration properties and the exclusion of blazars are both expected to be related mainly to our viewing angle to these AGN (e.g., Antonucci, 1993), which is not dependent on the spin of their central SMBHs. The Eddington ratio selection relates specifically to the accretion rate onto the AGN "today", while the spin of the SMBH will be mainly determined by its long-term growth history instead. Indeed, the Horizon-AGN simulation shows no connection between SMBH spin and the instantaneous accretion rate in the analysed snapshot. Finally, the reflection fraction selection still permits spins across the full range of possible prograde spin values ($a* = 0$–0.998), as even Schwarzschild black holes ($a* = 0$) should result in reflection from the disc with $R \geq 1$ if the disc reaches the ISCO (e.g., Dauser et al., 2016).

Our various cuts leave a sample of 192 AGN from BASS for which spin measurements should be possible. All of these sources are relatively local, with a median redshift of $z \sim 0.05$ (see "BASS parent" in the right panel of Figure 4), consistent with the $z = 0.0556$ snapshot of the Horizon-AGN simulation we use in this work. Conveniently, these sources all have an estimate of M_{BH}, among which ~80% are based on single-epoch virial Hβ and Hα estimators, ~8% on the $\boldsymbol{M_{\mathrm{BH}} - \sigma*}$ relation and the remaining ~12% are drawn from reverberation mapping and resolved stellar and gas dynamics published in the literature. Together, the 192 AGN span a broad range of black hole masses, $5.5 \lesssim \log(M_{\mathrm{BH}}/\mathrm{M}_\odot) \lesssim 10.0$ (middle and left panels in Figure 4), which is well suited to placing constraints on different potential black hole growth models. The sample is also particularly appropriate for comparisons against Horizon-AGN specifically, with the M_{BH} distribution in our parent BASS sample showing good qualitative agreement with the black holes extracted from the cosmological simulation (left panel in Figure 4). Finally, we note that while targeting all hard X-ray detected *Swift*-BAT AGN, the BASS survey is not designed to probe a representative sample of mass assembly histories of their galactic hosts. In consequence, our BASS parent sample may not be perfectly representative of all SMBH growth channels present in the observable Universe.

7 Sample size and spin uncertainty requirements

In order to design observational strategies for differentiating between SMBH growth scenarios with spin parameter measurements, we need to establish the sample size and maximum spin measurement uncertainty (σ_{a*}) necessary for such work. Both requirements are imposed by a combination of two independent factors: the difference between the SMBH growth history models as a function of mass in Horizon-AGN, and the SMBH mass distribution of our parent BASS sample (Section 6.1). In order to determine these requirements, below we simulate a set of potential survey programmes covering a range of realistic measurement uncertainties and sample sizes.

7.1 Simulating realistic samples informed by Horizon-AGN

Figure 2 shows that the two SMBH growth scenarios separate in the $M_{\mathrm{BH}} - a*$ plane above $10^8 \mathrm{M}_\odot$, with the strongest difference at the high-M_{BH} end. It is also apparent that at high masses the accretion + mergers distribution (orange) spans a broad range in spin parameter values. Therefore, in order to differentiate between the two growth scenarios with realistic samples, we base our strategy on a simple statistical approach—discretising the spin–mass plane by calculating sample means in bins of M_{BH}. This way we can both reduce the impact of the uncertainty on individual $M_{\mathrm{BH}} - a*$ measurements and coarsely capture the two-dimensional trends which would otherwise require large sample

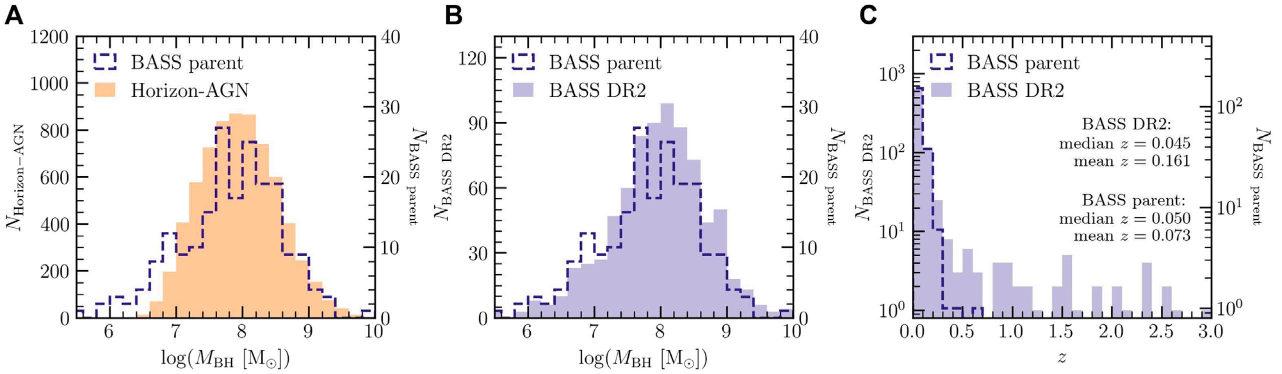

FIGURE 4
(A): comparison of SMBH mass distributions between our parent BASS sample (BASS parent, Section 6.1 and the Horizon-AGN cosmological simulation, demonstrating good agreement between potential AGN targets and the cosmological model. **(B)**: M_{BH} comparison between the whole BASS catalogue (BASS DR2) and out parent BASS sample. The distributions in M_{BH} are comparable, demonstrating that our sample selection criteria do not introduce additional bias with respect to the full BASS DR2 catalogue. **(C)**: comparison of redshift distributions between our parent BASS sample and the full BASS DR2 AGN catalogue sources. As expected, our sample selection removes the highest-redshift sources. However, the median redshift remains comparable at $z =$ 0.05.

sizes for a direct comparison between 2D distributions. To best capture the signal we select one bin below $M_{\mathrm{BH}} = 10^8 \mathrm{M}_\odot$ (where both scenarios make consistent predictions) and for higher masses we split the sample into two bins above and below $\log(M_{\mathrm{BH}}/\mathrm{M}_\odot) = 8.7$ ($M_{\mathrm{BH}} \approx 5 \times 10^8 \mathrm{M}_\odot$). This choice is motivated by the SMBH mass distribution shown in the left panel of Figure 4; there are 9 AGN with $\log(M_{\mathrm{BH}}/\mathrm{M}_\odot) > 8.7$ among the brightest 100 X-ray sources in the 2–10 keV band in our parent BASS selection (which we consider as an initial plausible sample size), which yield a Poisson signal-to-noise ratio of 3 for source number count in the highest mass bin. On the low-mass end we restrict the mass bin to $M_{\mathrm{BH}} > 10^6 \mathrm{M}_\odot$ to match the Horizon-AGN M_{BH} distribution. Our final binning scheme results in the following ranges in $\log(M_{\mathrm{BH}}/\mathrm{M}_\odot)$ [6.0, 8.0] [8.0, 8.7] and [8.7, 10.0].

By estimating mean $a*$ values, we take advantage of the $\sqrt{N}$ scaling with sample size N of the standard error on the mean, which allows us to clearly separate the two SMBH growth scenarios in the coarsely binned $M_{\mathrm{BH}} - a*$ plane. With M_{BH} ranges in place, we can now determine the minimum sample size and uncertainty required for a series of mean $a*$ measurements to differentiate between the orange and blue SMBH populations in Figure 2. We proceed by selecting the K brightest sources from our parent BASS sample for a set of different values for K, thus imposing a single X-ray flux limit across the whole range in SMBH mass in each case. This way we match the assumptions discussed earlier in Section 4 and hence can implement the radiative efficiency - spin parameter bias expected for flux-limited AGN samples in the local Universe. We then extract $a*$ distributions for both SMBH growth histories in each M_{BH} bin from Horizon-AGN and correct them for the $\eta(a*)$ bias (see Supplementary Appendix S1 for details).

To simulate realistic samples of AGN, we take a total of $K = \Sigma K_i$ random draws from the bias-corrected spin distributions across all M_{BH} bins, with the sample sizes K_i in each individual bin determined by the number of BASS sources which fall within this SMBH mass range[11], among the K brightest AGN from our selection in Section 6.1. We perform the spin draws separately for each SMBH growth model, and hence for each realization of a potential observational sample of a total of K AGN, we have a paired set of predicted spin values for the accretion-only and accretion + mergers growth models. To simulate the effect of measurement uncertainty we then perturb the spin values drawn above by further random draws from a normal distribution $N(0, \sigma_{a*})$, where σ_{a*} is the assumed uncertainty on the spin measurements[12], and where we consider a range of values for σ_{a*}. For each a_i^*, the normal distribution is singly truncated at $\sigma_i = (0.998 - a_i^*)/\sigma_{a*}$ to account for the theoretical upper limit on the spin parameter of $a* = 0.998$. This way, each potential AGN sample from a given SMBH growth history consists of K spin measurements expected from $\eta(a*)$ bias-corrected Horizon-AGN distributions, post-processed to account for measurement uncertainty.

As a final step in each simulated AGN sample, for each mass bin we calculate the mean spin value together with its corresponding standard error on the mean: $\mu_{\mathrm{acc}} \pm \delta_{\mathrm{acc}}$ for the accretion-only scenario and $\mu_{\mathrm{acc+mer}} \pm \delta_{\mathrm{acc+mer}}$ for accretion + mergers. To calculate the standard error, we necessarily assume that each paired draw consists of $a*$ measurements without lower limits in both SMBH growth histories. However, we note that some lower limits are likely to be present in real observations. Finally, we check the probability of the two mean measurements in a mass bin Ω being drawn from the same underlying distribution by calculating the right-tail p-value

---

[11] Throughout the study we treat the three sources with $M_{\mathrm{BH}} < 10^6 \mathrm{M}_\odot$ in the parent BASS sample as belonging to the lowest mass bin, given the large uncertainty associated with low M_{BH} estimates.

[12] Note that at this point we simply assume all spin measurements to have the same uncertainty; more realistic scenarios that include the expected dependence of measurement uncertainties as a function of spin are investigated in Section 9.

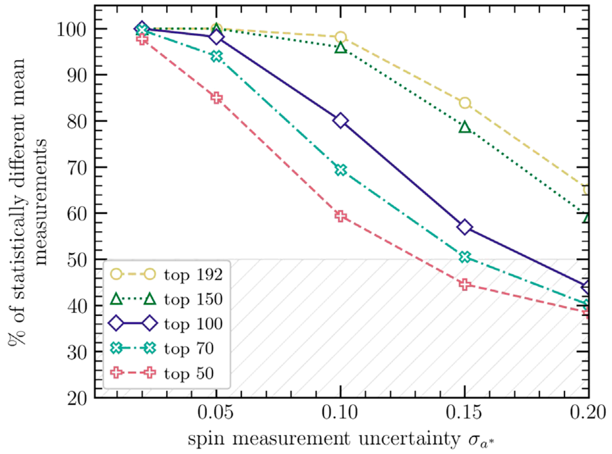

FIGURE 5
Minimum spin measurement uncertainty (σ_{a^*}) and sample size required for simulated observations to differentiate between accretion-only and merger and accretion SMBH growth scenarios drawn from the HorizonAGN cosmological simulation. Individual curves show the simulated observations performed for the top 50, 70, 100, 150 and 192 brightest X-ray sources in the 2–10 keV band in our parent BASS sample. In order for a median (50th percentile) simulated measurement to tell SMBH growth histories apart, one requires Gaussian spin measurement uncertainty of $\lesssim 0.15$ across the entire range in $a*$ for a sample of 70 sources.

(p_Ω) of $\mu_{\mathrm{acc}} - \mu_{\mathrm{acc+mer}}$ belonging to $N(0, \sqrt{\delta_{\mathrm{acc}}^2 + \delta_{\mathrm{acc+mer}}^2})$. In this way, we calculate the probability that a given paired set of predicted spin values in a bin cannot differentiate between the accretion-only and accretion + mergers growth scenarios. For our simulated AGN samples, we consider spin measurement uncertainties in the range $\sigma_{a^*} \in [0.02, 0.05, 0.10, 0.15, 0.20]$, and sample sizes of $K \in [50, 70, 100, 150, 192]$. For each combination of these values we repeat the above process 10^4 times, generating a large set of potential AGN samples, together with their corresponding mean spin parameter measurements as a function of mass.

Figure 5 shows the fraction of these simulated AGN samples which result in a statistically different measurement of mean spin parameter value between the accretion-only and accretion + mergers SMBH growth scenarios as a function of $a*$ measurement uncertainty and sample size. In order to take full advantage of the difference between the two predictions at high SMBH masses, in each realization of a potential AGN sample we combine the results for both of the mass bins with $M_{\mathrm{BH}} > 10^8 \mathrm{M}_\odot$. Since these can be treated as independent measurements, the combined probability of the simulated accretion-only and accretion + mergers samples being drawn from the same distribution in the $M_{\mathrm{BH}} - a*$ plane for *both* mass bins becomes $p_{\mathrm{total}} = p_{[8,8.7]} \times p_{[8.7,10]}$. The vertical axis in Figure 5 shows the fraction of simulated measurements which result in $p_{\mathrm{total}} < 0.01$ as a function of σ_{a^*} in the x-axis. Different lines and markers correspond to the top 192, 150, 100, 70 and 50 brightest AGN in our parent BASS sample. Whenever the curves enter the gray hatched region, the median measurement expected from the 10^4 realizations of potential AGN samples will not differentiate between the accretion-only and accretion + mergers BH growth scenarios.

As expected, Figure 5 shows that increasing the uncertainty on individual spin measurements at fixed sample size decreases the fraction of simulated samples capable of differentiating between the two SMBH growth histories. Similarly, at fixed uncertainty, a larger sample size results in higher chances for a single realization of such a sample to tell the two growth histories apart. In the context of minimum survey requirements, we find that for a sample size of >70 AGN we would need a maximum of $\sigma_{a^*} \lesssim 0.15$ for a median expected measurement to differentiate between the accretion-only and accretion + mergers SMBH populations. In order to be conservative, we therefore suggest that a sample size of $K = 100$ AGN drawn from our BASS selection with spins measured to a precision of $\sigma_{a^*} \leq 0.15$ would be sufficient to distinguish between these different SMBH growth scenarios.

8 *HEX-P* simulations

Given the importance of simultaneous broadband X-ray spectroscopy for providing observational constraints on SMBH spin, a mission with the profile of *HEX-P* is ideally suited to building the significant samples of SMBH spin measurements required to finally connect these measurements to cosmological BH growth models. We now present a set of simulations that showcase the anticipated capabilities of *HEX-P* in this regard.

8.1 Mission design

The Low Energy Telescope (LET) onboard *HEX-P* consists of a segmented mirror assembly coated with Ir on monocrystalline silicon that achieves a half power diameter of 3.5″, and a low-energy DEPFET detector, of the same type as the Wide Field Imager (WFI; Meidinger et al., 2020) onboard Athena (Nandra et al., 2013). It has 512 × 512 pixels that cover a field of view of 11.3′ × 11.3′. It has an effective passband of 0.2–20 keV, and a full frame readout time of 2 ms, which can be operated in a 128 and 64 channel window mode for higher count-rates to mitigate pile-up by allowing a faster readout. Pile-up effects remain below an acceptable limit of ~ 1% for fluxes up to ~ 100 mCrab in the smallest window configuration (64w). Excising the core of the PSF, a common practice in X-ray astronomy, allows for observations of brighter sources, with a typical loss of up to ~ 60% of the total photon counts.

The High Energy Telescope (HET) consists of two co-aligned telescopes and detector modules. The optics are made of Ni-electroformed full shell mirror substrates, leveraging the heritage of *XMM-Newton*, and coated with Pt/C and W/Si multilayers for an effective passband of 2–80 keV. The high-energy detectors are of the same type as flown on *NuSTAR*, and they consist of 16 CZT sensors per focal plane, tiled 4 × 4, for a total of 128 × 128 pixel spanning a field of view of 13.4′ × 13.4′.

8.2 Instrumental responses

All the mission simulations presented here were produced with a set of response files that represent the observatory performance based on current best estimates as of spring 2023 (see Madsen et al. 2023). The effective area is derived from raytracing calculations for the mirror design including obscuration by all known structures. The detector responses are based on simulations performed by the respective hardware groups, with an optical blocking filter for the LET and a Be window and thermal insulation for the HET. The LET background was derived from a GEANT4 simulation (Eraerds et al., 2021) of the WFI instrument, and the background simulation for the HET was derived from a GEANT4 simulation of the *NuSTAR* instrument. Both simulations adopt the planned L1 orbit of *HEX-P*. The broad X-ray passband and superior sensitivity will provide a unique opportunity to study accretion onto SMBHs across a wide range of energies, luminosities, and dynamical regimes.

8.3 Spectral simulations

To assess the ability of *HEX-P* to constrain black hole growth models via AGN spin measurements, we perform a series of spectral simulations covering a range of spin values relevant to the cosmological simulations discussed above: $a* = 0.5, 0.7, 0.9, 0.95$. We first focus on the lowest spin value among this set, $a* = 0.5$, and perform a set of simulations at different exposures in the range 50–200 ks. For each exposure, we simulate 100 different spectra using the above response files and the XSPEC spectral fitting package (v12.11.1; Arnaud, 1996) in order to determine the minimum exposure that provides the *HEX-P* data quality needed for an average 1σ constraint on the spin of $\sigma_{a*} \leq 0.15$, as required above. We then perform further sets of 100 simulations with this exposure for each of the spin values listed above to map out the expected uncertainty as a function of input spin (as it is well-established that for a given observational setup, tighter constraints are obtained for higher spin values, e.g., Bonson and Gallo, 2016; Choudhury et al., 2017; Kammoun et al., 2018; Barret and Cappi, 2019).

We make use of the RELXILL family of disk reflection models (Dauser et al., 2014; García et al., 2014) for these simulations, and construct a spectral model that draws on the typical properties of the 192 BASS AGN selected above (Section 6.1), general expectations for the unobscured AGN selected based on the unified model for AGN, and typical results seen from AGN for which detailed reflection studies have already been possible in the literature. We specifically make use of the RELXILLLPCP model, which assumes a simple lamppost geometry for the corona, and that the ionizing continuum is a thermal Comptonization model (specifically the NTHCOMP model; Zdziarski et al., 1996; Zycki et al., 1999).

For the key model parameters, we assume the spectrum of the primary continuum has parameters $\Gamma = 2.0$ and $kT_e = 100$ keV for the photon index and electron temperature, respectively, relatively typical parameters for unobscured AGN (Ricci et al., 2017; Baloković et al., 2020). This illuminates a geometrically thin accretion disk which is assumed to extend down to the ISCO. AGN with moderate-to-low levels of obscuration are generally expected to be viewed at moderate-to-low inclinations in the unified model (Antonucci, 1993), so we assume an inclination of 45°. The disk is assumed to be ionized, with an ionization parameter[13] of $\log[\xi/(\mathrm{erg cm s})] = 2$ (typical of values reported from relativistic reflection analyses in the literature, e.g., Ballantyne et al., 2011; Walton et al., 2013; Jiang et al., 2019; Mallick et al., 2022), and to have solar iron abundance (i.e., $A_{\mathrm{Fe}} = 1$). We assume the corona has a height of $h = 5R_{\mathrm{G}}$ for the $a* = 0.5$ simulations, and then that it has constant height in vertical horizon units as we subsequently vary the spin. This is equivalent to assuming the scale of the corona contracts slightly as the inner radius of the disk moves inwards, as might be expected should the corona be related to magnetic reconnection around the inner disk (e.g., Merloni and Fabian, 2001); in gravitational radii, these coronal heights correspond to values in the range ~4–5 R_{G}, which are relatively standard values inferred for the sizes of X-ray coronae (e.g., De Marco et al., 2013; Reis and Miller, 2013; Kara et al., 2016; Mallick et al., 2021). The reflection fraction is calculated self-consistently based on the combination of $a*$ and h, both when computing the simulations and also when subsequently fitting the simulated data to explore constraints on $a*$.

As we need a sample of ~100 AGN to distinguish the black hole growth models, we normalize all of our simulations to have a 2–10 keV flux of 6×10^{-12} erg cm^{-2} s^{-1}, corresponding to the flux of the 100th brightest source in the sample of AGN selected above (see Section 6.1). At this flux level, we find that a *HEX-P* exposure of 150 ks is required to provide an average uncertainty of $\sigma_{a*} \leq 0.15$ for an input spin value of $a* = 0.5$. We also find that, as broadly expected, the typical uncertainty on the spin measurements *HEX-P* will decrease for more rapidly rotating black holes (see Figure 6). Although our results do differ quantitatively to the prior efforts that have also come to similar conclusions, the overall quantitative trend we find is consistent with these previous works (e.g., Bonson and Gallo, 2016; Kammoun et al., 2018). These quantitative differences mainly relate to the fact that we are simulating *HEX-P* spectra instead of *XMM-Newton* + *NuSTAR* spectra, with some contribution from the fact that different model versions and slightly different assumptions are used here. An example spectrum from one of our simulations for $a* = 0.9$ is shown in Figure 7, along with the projected constraints on $a*$, h and source inclination i for that simulation.

9 Constraining SMBH growth channels with *HEX-P*

Having established the minimum survey requirements, we now demonstrate *HEX-P*'s ability to differentiate between accretion-only and accretion + mergers SMBH growth scenarios. To this end we repeat the simulations introduced in Section 7.1 for the brightest 100 sources in the parent BASS sample (Section 6.1), this time replacing the constant spin parameter uncertainty σ_{a*} assumed previously with the $a*$-dependent uncertainties $\sigma(a*)$ obtained from spectral simulations in Section 8.3 (see Figure 6), i.e., now specifically simulating observational campaigns with *HEX-P*. Similarly to our initial tests, we simulate 10^4 paired AGN

---

[13] The ionization parameter has its usual definition of $\xi = L/nR^2$, where L is the ionizing luminosity, n is the number density of the plasma, and R is the distance between the plasma and the ionizing source

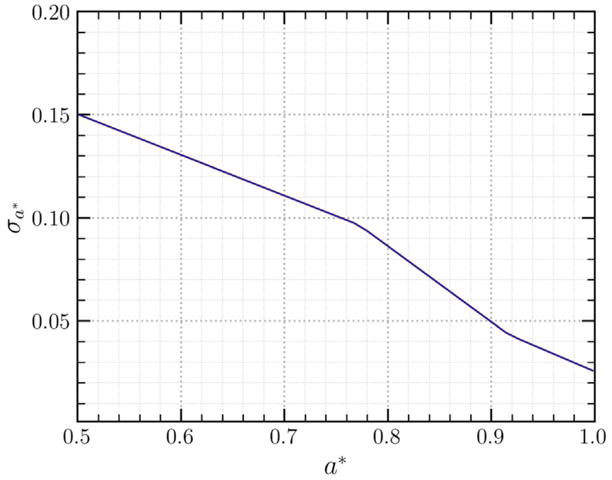

FIGURE 6
Spin parameter measurement uncertainty $\sigma(a*)$ vs. spin parameter $a*$, extracted from the *HEX-P* spectral simulations of relativistic reflection in AGN discussed in Section 8.3 (which assume a 2–10 keV flux of 6×10^{-12} erg cm^{-2} s^{-1} and an exposure time of 150 ks).

samples to assess the probability with which *HEX-P* will confidently discriminate between SMBH growth histories.

Figure 8 illustrates the observational constraints that would be expected for one such paired set of simulated AGN samples, randomly selected from our set of simulations, comparing the accretion-only (blue circles) and accretion + mergers (orange squares) SMBH growth scenarios against the current spin parameter constraints for $M_{\rm BH} > 10^6 {\rm M}_\odot$ (gray diamonds). In order to account for the existence of lower limits expected in realistic measurements, by analogy with the measurements collected from the literature, we use open symbols to indicate right-censored spin draws, i.e., a_i^* for which $0.998 - a_i^* < \sigma(a_i^*)$. Vertical error bars mark 1σ uncertainties in both simulated and existing $M_{\rm BH} - a*$ constraints, allowing for a direct comparison between the two. All BASS $M_{\rm BH}$ measurements in the figure are assigned a **± 0.5 *dex*** uncertainty expected for their estimate via the single-epoch virial method (Shen, 2013). Figure 8 demonstrates the potential for such a *HEX-P* spin measurement campaign to map the spin-mass plane with unprecedented accuracy. In comparison with currently available constraints, the *simulated observations offer clear improvements in measurement precision, control of sample selection biases, and a greater than twofold increase in sample size*.

Moving on from an individual realization, the top panels in Figure 9 present the distribution of mean $a*$ measurements (μ) for the whole suite of 10^4 simulations for the accretion + mergers (orange) and accretion-only (blue) SMBH growth histories for the three bins of $M_{\rm BH}$. Vertical dashed lines mark μ at which each distribution peaks, indicating the most likely expected mean spin parameter measurement for each growth scenario. Similarly, bottom panels present the corresponding distributions of the standard errors on the mean (δ) together with their peaks marked with vertical dashed lines. The mean spin parameter values from Horizon-AGN together with their most likely measurements expected from *HEX-P* observations are summarized in Table 1.

Together, Figure 9 and Table 1 demonstrate the potential of mean $a*$ measurements in bins of $M_{\rm BH}$ for differentiating between the accretion-only and accretion + mergers SMBH growth scenarios within the Horizon-AGN cosmological model. As expected from Figure 2, the simulated constraints in the lowest mass bin are consistent between the two SMBH populations, but become statistically separable for $M_{\rm BH} > 10^8 {\rm M}_\odot$. In all three panels in Figure 9, the distributions of mean accretion-only measurements are narrower than the accretion + mergers distributions, with consistently high peak values matching the true $\eta(a*)$ bias-corrected mean $a*$ in Horizon-AGN to within <2%. The orange distributions, on the other hand, peak at progressively lower values with increasing $M_{\rm BH}$, following the trend expected from the cosmological simulation to within <2% as well. We also note that the simulated accretion + mergers mean spin measurements form a visibly left-skewed distribution, primarily owing to the progressive spin parameter uncertainty prescription in our simulations which assumes larger σ_{a*} for lower spin values based on our *HEX-P* spectral simulations (Section 8.3)[14]. The middle mass bin shows a non-neglible overlap between the accretion-only and accretion + mergers distributions, with their two peaks clearly separated by $\Delta_\mu \simeq 0.03$. For $\log(M_{\rm BH}/{\rm M}_\odot) > 8.7$ the two SMBH growth scenarios form nearly non-overlapping distributions with peak mean spin parameter values separated by $\Delta_\mu \simeq 0.16$, despite the modest number of only 9 BASS sources available in the mass bin. We note, however, that small sample statistics do lead to a significant spread in the simulated values for accretion + mergers scenario.

In Figure 10 we summarize the prospects for constraining the cosmic growth history of SMBHs via X-ray reflection spectroscopy with a *HEX-P* spin survey similar to the design outlined above. The figure shows the expected mean $a*$ measurements in three bins of $M_{\rm BH}$ for accretion-only (blue circles) and accretion + mergers (orange squares) scenarios, inferred from our suite of simulated observations of the brightest 100 AGN in our parent BASS sample. The y-axis locus of individual points correspond to the vertical dashed lines in the top panels of Figure 9, while the length of the error bars correspond to the vertical dashed lines in the bottom panels. Since it is likely that observations of high-$a*$ SMBHs will result in a significant fraction of constraints that are lower limits, we mark the prediction for the accretion-only growth scenario as a lower limit. We also compare the results of our simulations to the current constraints, showing mean spin parameter values in identical mass bins for $M_{\rm BH} - a*$ measurements calculated earlier in Section 4.1 (and presented earlier in Figure 2).

Figure 10 clearly demonstrates that *future HEX-P spin measurements will allow us to differentiate between the two SMBH growth channels as inferred from the Horizon-AGN cosmological model*. The expected mean measurements in the highest mass bin alone reject the null hypothesis of the accretion-only and accretion + mergers results being drawn from the same distribution at the level of 2.8σ ($p_{[8.7-10.0]} = 2.5\times10^{-3}$). Across the whole suite of our simulations, >82% (>36%) of paired simulated measurements in the highest mass bin reject the null hypothesis at $>2\sigma$ ($>3\sigma$) confidence

---

[14] The skewness is also present in the accretion-only scenario, however, this effect is less visibly apparent due to the narrow width of the distribution.

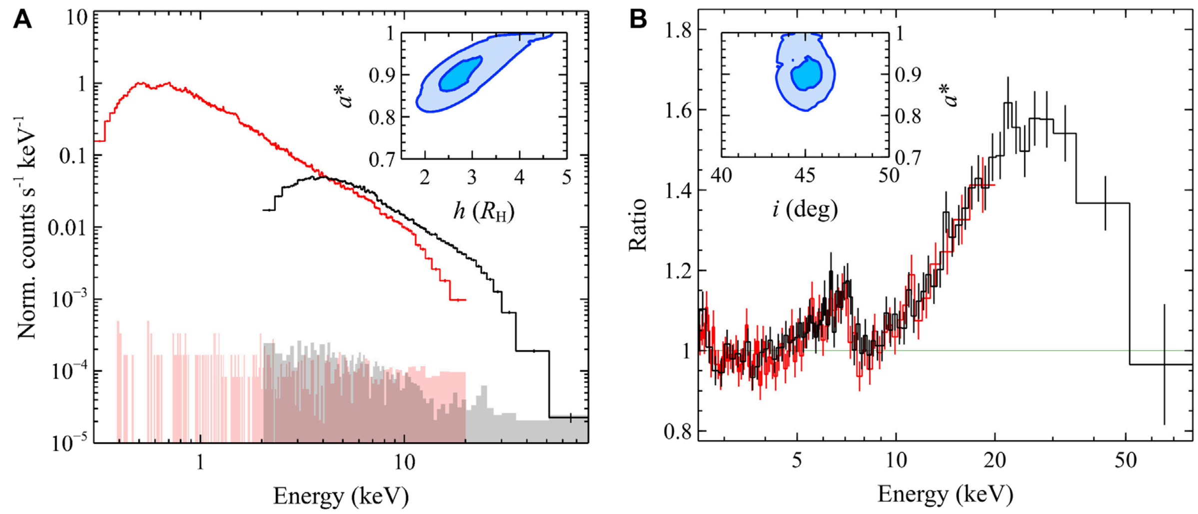

FIGURE 7
(A): Count spectra for the LET (red) and the HET (black) for one of our *HEX-P* spectral simulations with $a* = 0.9$, along with their corresponding instrumental backgrounds (shaded regions). **(B)**: The same simulated spectra plotted as a ratio to a simple CUTOFFPL continuum model (a powerlaw with an exponential high-energy cutoff), fit to the 2–4, 8–10 and 50–80 keV bands (where the primary continuum would be expected to dominate). We zoom in on the data above 2 keV to highlight the key reflection features: the relativistically broadened Fe Kα peaking at ~6–7 keV and the Compton hump peaking at ~30 keV. The two insets show the projected constraints on $a*$, h and source inclination i for this simulation (displayed as 2-D confidence contours, with the 1σ and 2σ levels shown).

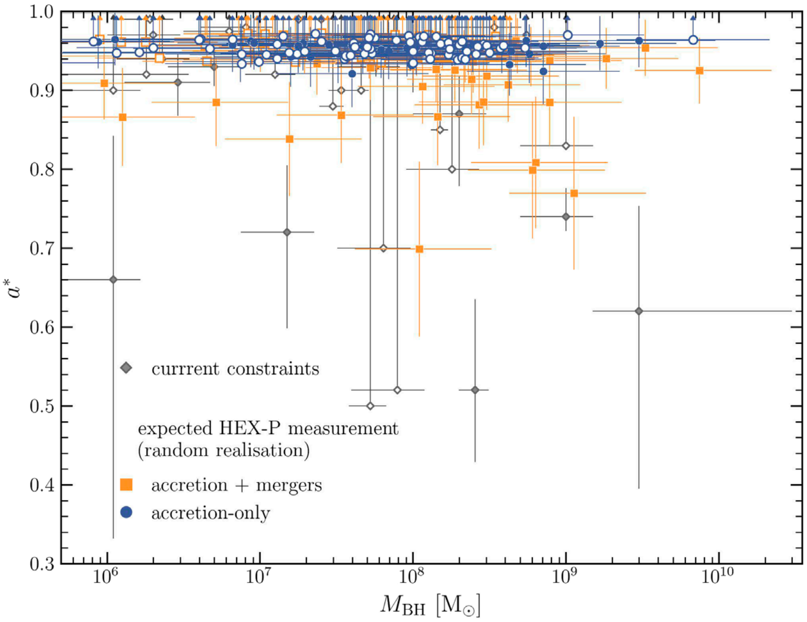

FIGURE 8
Comparison between current published constraints (grey diamonds) and a random realization of simulated *HEX-P* measurements for the accretion-only (blue circles) and accretion + mergers SMBH growth scenarios (orange squares). Empty symbols show lower limits on $a*$, while filled symbols denote measurements with vertical errorbars marking their corresponding 1σ confidence ranges. With its expected spin measurement uncertainty, *HEX-P will provide unprecedented constraints on the $M_{\rm BH} - a*$ plane for SMBHs in the local Universe.*

level. When we combine the measurements for both mass bins above $10^8 M_\odot$ in SMBH mass, the expected *HEX-P* measurement can differentiate between the two growth histories at ~4.3σ and across all simulated measurements at >3σ (>4σ) confidence level in >88% (>65%) of all paired draws. Figure 10 also illustrates that the current spin constraints are not yet sufficient to make the distinction between these different growth scenarios; a dedicated SMBH spin survey with improved individual constraints, a larger sample size

TABLE 1 Summary of mean spin parameter values in simulated *HEX-P* observations and Horizon-AGN.

$\log(M_{\rm BH}/{\rm M}_\odot)$ bin		[6.0, 8.0]	[8.0, 8.7]	[8.7, 10.0]
Horizon-AGN	accretion-only	0.996	0.993	0.993
	accretion + mergers	0.959	0.905	0.768
Horizon-AGN	accretion-only	0.996	0.995	0.995
with $\eta(a*)$ bias	accretion + mergers	0.981	0.953	0.851
Expected measurement	accretion-only	0.977 ± 0.002	0.975 ± 0.003	0.976 ± 0.005
	accretion + mergers	0.966 ± 0.004	0.945 ± 0.011	0.86 ± 0.04

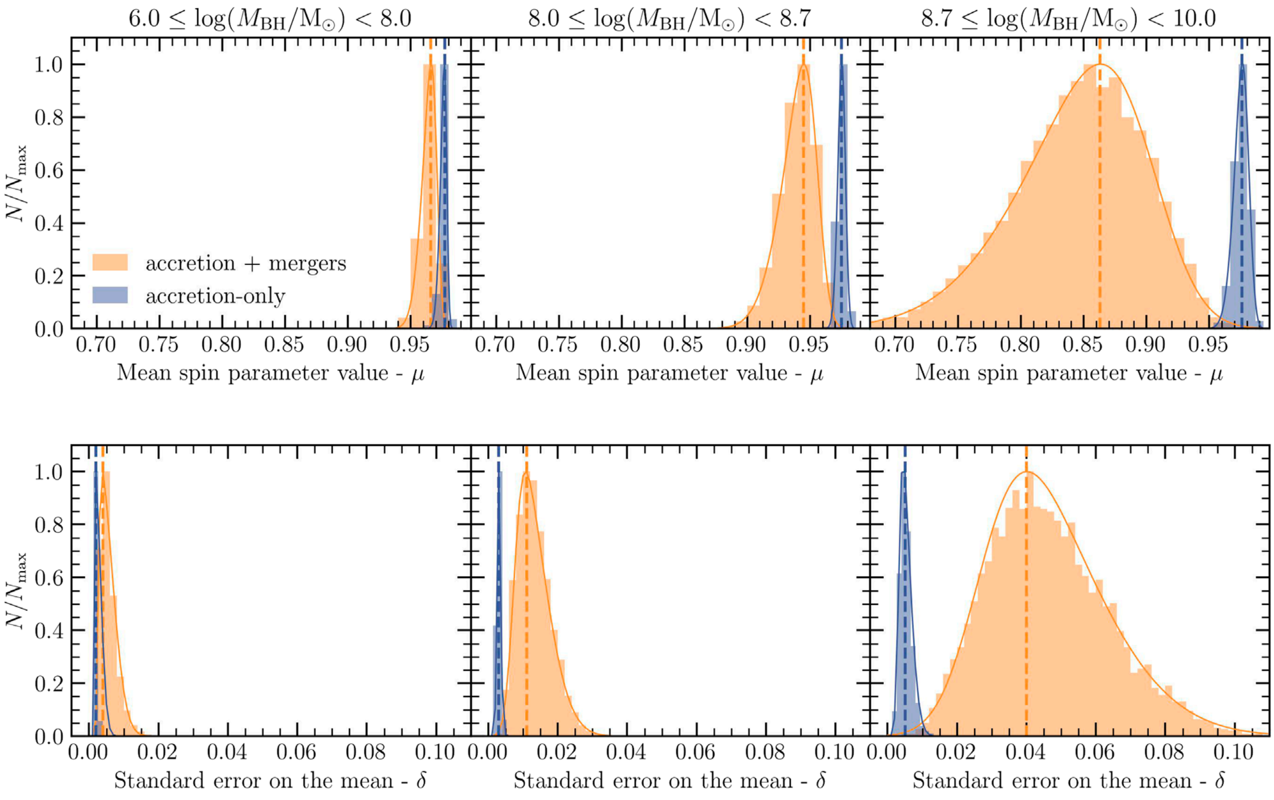

FIGURE 9
Summary of mean spin parameter estimates for 10^4 realisations of simulated *HEX-P* observing campaigns. **(A)**: distribution of expected mean $a*$ estimates (μ) in bins of $M_{\rm BH}$ for accretion-only (blue) and accretion + mergers (orange) SMBH growth scenarios. **(B)**: corresponding distributions of the standard errors on the mean (δ). Peak locations in each distribution are marked with vertical dashed lines. Differences between the mean spin measurements for the two scenarios become apparent for $M_{\rm BH} > 10^8 {\rm M}_\odot$ with the most massive bin showing the strongest signal.

and well-controlled biases—similar to the one envisioned here for *HEX-P*—is required to drive the combined SMBH spin constraints towards distinguishing the models.

10 Final remarks

We have shown that a sample of 100 AGN with the data quality determined in Section 7 and the mass distribution of the 100 brightest sources in our BASS selection (Section 6.1) is sufficient to distinguish between different cosmological SMBH growth scenarios. We now assess the level of observational investment from *HEX-P* that would be required to achieve this result. Given that a 150 ks *HEX-P* exposure provides the necessary data quality for our required spin constraints ($\sigma_{a*} \le 0.15$ for $a* = 0.5$) for a source with a 2–10 keV flux of 6×10^{-12} erg cm^{-2} s^{-1}, we calculate a rough estimate for how long it would take for *HEX-P* to provide this level of data quality for all 100 sources by scaling this 150 ks

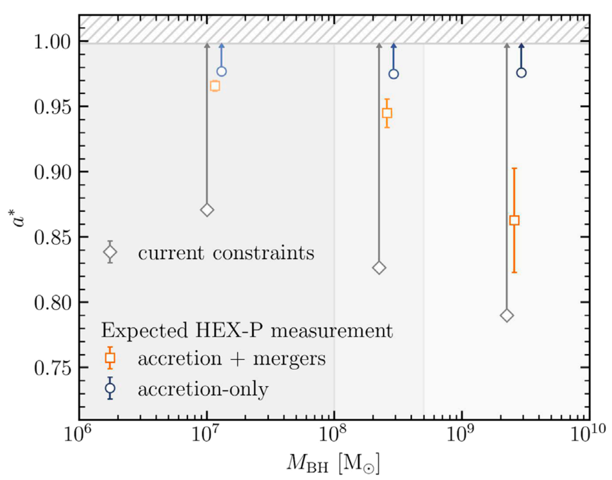

FIGURE 10
Comparison of mean spin parameter measurements in bins of M_{BH} between published constraints (grey diamonds) and expected *HEX-P* measurements for accretion-only (blue circles) and accretion + mergers (orange squares) SMBH growth scenarios. For *HEX-P* measurements we show the most likely result from our simulations, corresponding to the vertical dashed lines in Figure 9. Background shading marks our M_{BH} binning scheme, while the gray hatching at the top indicates the spin parameter range forbidden by the Thorne (1974) limit. The expected *HEX-P spin parameter measurements will allow us to differentiate between SMBH growth histories*, unlike $M_{\mathrm{BH}} - a*$ constraints placed until now.

exposure to the actual observed 2–10 keV flux for each source (as reported in the BASS catalogue). Formally, this is a slightly conservative approach, as the instrumental background will make a smaller contribution for higher source fluxes, though even for the faintest sources, the background only impacts the highest energies probed by each detector (see Figure 7), so this simplification will only have a minimal effect across this sample. Summing the exposure required for each of the brightest 100 sources, we find that a total observing investment of ~10 Ms from *HEX-P* is necessary.

While this is a significant investment, it is a program that is achievable when spread over the full 5-year lifetime of *HEX-P*. This unique capability highlights *HEX-P*'s transformative nature as a next-generation X-ray observatory, allowing it to complete large observing programs otherwise unfeasible with coordinated exposures between separate hard and soft X-ray facilities. Collecting a sample of a 100 SMBH spin parameter measurements from *NuSTAR* observations combined with a soft X-ray observatory would require no less than 30 years to complete, given $\boldsymbol{a}*$ publication trends since the mission's launch (see Figure 1 in Madsen et al. 2023). The strictly simultaneous broadband X-ray coverage of *HEX-P*, critical for SMBH spin parameter recovery, would render a large sample size straightforward to achieve, owing to flexible scheduling absent multi-facility coordination restrictions. In particular, a spin survey such as this could serve a similar function to the *HEX-P* mission as the ongoing *Swift*/BAT survey conducted by *NuSTAR* (e.g., Baloković et al., 2020). This program gradually builds up *NuSTAR* observations of hard X-ray sources detected by the *Swift*/BAT detector via regular scheduling of short "filler" observations within the primarily Guest Observer program. Indeed, even the longest exposures required here–150 ks – could be split into 3 × 50 ks observations for ease of scheduling. The regular inclusion of such observations in the schedule allows for increased flexibility to respond to transient phenomena (i.e., target-of-opportunity observations), as these survey observations can easily be rescheduled since they have no real time constraints and the simultaneity of the coverage across the full 0.2–80 keV bandpass is already guaranteed.

Most importantly, our study demonstrates that in the light of theoretical predictions delivered by state-of-the-art cosmological hydrodynamical simulations tracing SMBH spin evolution, only large statistical samples of consistent measurements are capable of isolating SMBH growth channels. Once radiative efficiency-spin bias is accounted for, the differences in statistical properties of SMBH populations in the $M_{\mathrm{BH}} - a*$ plane decrease in magnitude, requiring both high precision on individual measurements and numerous AGN observations at $M_{\mathrm{BH}} > 10^8 \mathrm{M}_\odot$ to constrain average trends in spin parameter as a function of SMBH mass. Although such measurements are, in principle, possible with currently available instruments, they critically require simultaneous observations with soft and hard X-ray observatories (e.g., *XMM-Newton* and *NuSTAR*). The necessary exposure time comparable to the expected *HEX-P* investment for these observatories renders such a study unfeasible due to the limitations associated with program allocation and scheduling conflicts among individual instruments.

Beyond distinguishing cosmological SMBH growth scenarios via spin measurements, the high-S/N broadband X-ray data generated by such a survey would provide a legacy for the *HEX-P* mission, and broader studies of AGN in general. For example, inner disk inclinations will be well constrained (see Figure 7), providing further tests of the broad applicability of the Unified Model (Antonucci, 1993) as well as allowing for additional sanity checks of the reflection results/searches for disk warps via comparison of these inclinations with constraints from the outer disk from, e.g., VLT/GRAVITY (see the cases of NGC3783 and IRAS 09149–2461, where the inner and outer disk inclinations from reflectionstudies and GRAVITY are in excellent agreement: Brenneman et al., 2011; Walton et al., 2020; GRAVITY Collaboration et al., 2020; GRAVITY Collaboration et al., 2021). These observations would also provide strong constraints on the X-ray corona for a large sample of AGN, both in terms of its location (see Figure 7) and its plasma physics via temperature measurements; all these observations will allow for important constraints on the electron temperature, facilitating further tests of coronal models (e.g., Fabian et al., 2015; see also Kammoun et al. 2023). All-in-all, while a program of this nature would be a major investment, the scientific return provided would be suitably vast.

Data availability statement

The raw data supporting the conclusions of this article will be made available by the authors, without undue reservation.

Author contributions

JP: Conceptualization, Formal Analysis, Investigation, Methodology, Visualization, Writing–original draft, Writing–review and editing. JG: Conceptualization, Funding acquisition, Investigation, Project administration, Resources, Writing–original draft, Writing–review and editing. DW: Conceptualization, Formal Analysis, Investigation, Methodology, Writing–original draft, Writing–review and editing. RB: Conceptualization, Data curation, Writing–review and editing. DS: Writing–review and editing. DB: Writing–review and editing. DW: Writing–review and editing. SB: Writing–review and editing. PB: Writing–review and editing. JB: Writing–review and editing. C-TC: Writing–review and editing. PC: Writing–review and editing. TD: Writing–review and editing. AF: Writing–review and editing. EK: Writing–review and editing. KM: Writing–review and editing. LM: Writing–review and editing. GiM: Writing–review and editing. GaM: Writing–review and editing. EN: Writing–review and editing. AP: Writing–review and editing. SP: Writing–review and editing. CR: Writing–review and editing. FT: Writing–review and editing. NT-A: Writing–review and editing. K-WW: Writing–review and editing.

Funding

The author(s) declare financial support was received for the research, authorship, and/or publication of this article. JP and JG acknowledge support from NASA grants 80NSSC21K1567 and 80NSSC22K1120. The work of DS was carried out at the Jet Propulsion Laboratory, California Institute of Technology, under a contract with NASA. CR acknowledges support from the Fondecyt Regular (grant 1230345) and ANID BASAL (project FB210003). LM acknowledges support from the CITA National Fellowship.

Acknowledgments

We would like to thank the anonymous referees for carefully reading the manuscript and for providing constructive comments which helped improve the quality of the paper. We would also like to acknowledge the journal editor, Renee Ludlam, recognizing her very smooth handling of the peer review process.

Conflict of interest

The authors declare that the research was conducted in the absence of any commercial or financial relationships that could be construed as a potential conflict of interest.

Publisher's note

Supplementary material

The Supplementary Material for this article can be found online at: https://www.frontiersin.org/articles/10.3389/fspas.2024.1324796/full#supplementary-material

References

Alexander, D. M., and Hickox, R. C. (2012). What drives the growth of black holes? *New Astron. Rev.* 56, 93–121. doi:10.1016/j.newar.2011.11.003

Alston, W. N., Fabian, A. C., Kara, E., Parker, M. L., Dovciak, M., Pinto, C., et al. (2020). A dynamic black hole corona in an active galaxy through X-ray reverberation mapping. *Nat. Astron.* 4, 597–602. doi:10.1038/s41550-019-1002-x

Annuar, A., Gandhi, P., Alexander, D. M., Lansbury, G. B., Arévalo, P., Ballantyne, D. R., et al. (2015). NuSTAR observations of the compton-thick active galactic nucleus and ultraluminous X-ray source candidate in NGC 5643. *Astrophysical J.* 815, 36. doi:10.1088/0004-637X/815/1/36

Antonucci, R. (1993). Unified models for active galactic nuclei and quasars. *ARA&A* 31, 473–521. doi:10.1146/annurev.aa.31.090193.002353

Arévalo, P., Bauer, F. E., Puccetti, S., Walton, D. J., Koss, M., Boggs, S. E., et al. (2014). The 2-79 keV X-ray spectrum of the circinus galaxy with NuSTAR, XMM-Newton, and chandra: a fully compton-thick active galactic nucleus. *Astrophysical J.* 791, 81. doi:10.1088/0004-637X/791/2/81

Arnaud, K. A. (1996). "XSPEC: the first ten years," in *Astronomical data analysis software and systems V*. Editors G. H. Jacoby, and J. Barnes (San Francisco: Astron. Soc. Pac.), 17.

Athanassoula, E., Bienayme, O., Martinet, L., and Pfenniger, D. (1983). Orbits as building blocks of a barred galaxy model. *A&A* 127, 349–360.

Avara, M. J., McKinney, J. C., and Reynolds, C. S. (2016). Efficiency of thin magnetically arrested discs around black holes. *MNRAS* 462, 636–648. doi:10.1093/mnras/stw1643

Ballantyne, D. R., McDuffie, J. R., and Rusin, J. S. (2011). A correlation between the ionization state of the inner accretion disk and the Eddington ratio of active galactic nuclei. *Astrophysical J.* 734, 112. doi:10.1088/0004-637X/734/2/112

Baloković, M., Harrison, F. A., Madejski, G., Comastri, A., Ricci, C., Annuar, A., et al. (2020). NuSTAR survey of obscured swift/BAT-selected active galactic nuclei. II. Median high-energy cutoff in seyfert II hard X-ray spectra. *Astrophysical J.* 905, 41. doi:10.3847/1538-4357/abc342

Bambi, C. (2017). *Black holes: a laboratory for testing strong gravity*. Singapore: Springer Nature. doi:10.1007/978-981-10-4524-0

Bambi, C., Brenneman, L. W., Dauser, T., García, J. A., Grinberg, V., Ingram, A., et al. (2021). Towards precision measurements of accreting black holes using X-ray reflection spectroscopy. *Space Sci. Rev.* 217, 65. doi:10.1007/s11214-021-00841-8

Barausse, E., and Rezzolla, L. (2009). Predicting the direction of the final spin from the coalescence of two black holes. *Astrophysical J.* 704, L40–L44. doi:10.1088/0004-637X/704/1/L40

Bardeen, J. M. (1970). Kerr metric black holes. *Nat* 226, 64–65. doi:10.1038/226064a0

Bardeen, J. M., Press, W. H., and Teukolsky, S. A. (1972). Rotating black holes: locally nonrotating frames, energy extraction, and scalar synchrotron radiation. *Astrophysical J.* 178, 347–370. doi:10.1086/151796

Barnes, J. E., and Hernquist, L. (1992). Dynamics of interacting galaxies. *ARA&A* 30, 705–742. doi:10.1146/annurev.aa.30.090192.003421

Barret, D., and Cappi, M. (2019). Inferring black hole spins and probing accretion/ejection flows in AGNs with the Athena X-ray Integral Field Unit. *A&A* 628, A5. doi:10.1051/0004-6361/201935817

Barthelmy, S. D., Barbier, L. M., Cummings, J. R., Fenimore, E. E., Gehrels, N., Hullinger, D., et al. (2005). The Burst Alert telescope (BAT) on the SWIFT midex mission. *Space Sci. Rev.* 120, 143–164. doi:10.1007/s11214-005-5096-3

Beckmann, R. S., Devriendt, J., Slyz, A., Peirani, S., Richardson, M. L. A., Dubois, Y., et al. (2017). Cosmic evolution of stellar quenching by AGN feedback: clues from the Horizon-AGN simulation. *MNRAS* 472, 949–965. doi:10.1093/mnras/stx1831

Beckmann, R. S., Smethurst, R. J., Simmons, B. D., Coil, A., Dubois, Y., Garland, I. L., et al. (2023). Supermassive black holes in merger-free galaxies have higher spins which are preferentially aligned with their host galaxy. *MNRAS* 527, 10867–10877. doi:10.1093/mnras/stad1795

Berti, E., and Volonteri, M. (2008). Cosmological black hole spin evolution by mergers and accretion. *Astrophysical J.* 684, 822–828. doi:10.1086/590379

Bîrzan, L., Rafferty, D. A., McNamara, B. R., Wise, M. W., and Nulsen, P. E. J. (2004). A systematic study of radio-induced x-ray cavities in clusters, groups, and galaxies. *Astrophysical J.* 607, 800–809. doi:10.1086/383519

Blandford, R. D., and McKee, C. F. (1982). Reverberation mapping of the emission line regions of Seyfert galaxies and quasars. *Astrophysical J.* 255, 419–439. doi:10.1086/159843

Blandford, R. D., and Znajek, R. L. (1977). Electromagnetic extraction of energy from Kerr black holes. *MNRAS* 179, 433–456. doi:10.1093/mnras/179.3.433

Bondi, H. (1952). On spherically symmetrical accretion. *MNRAS* 112, 195–204. doi:10.1093/mnras/112.2.195

Bondi, H., and Hoyle, F. (1944). On the mechanism of accretion by stars. *MNRAS* 104, 273–282. doi:10.1093/mnras/104.5.273

Bonson, K., and Gallo, L. C. (2016). How well can we measure supermassive black hole spin? *MNRAS* 458, 1927–1938. doi:10.1093/mnras/stw466

Bower, R. G., Benson, A. J., Malbon, R., Helly, J. C., Frenk, C. S., Baugh, C. M., et al. (2006). Breaking the hierarchy of galaxy formation. *MNRAS* 370, 645–655. doi:10.1111/j.1365-2966.2006.10519.x

Brenneman, L. W., and Reynolds, C. S. (2006). Constraining black hole spin via X-ray spectroscopy. *Astrophysical J.* 652, 1028–1043. doi:10.1086/508146

Brenneman, L. W., Reynolds, C. S., Nowak, M. A., Reis, R. C., Trippe, M., Fabian, A. C., et al. (2011). The spin of the supermassive black hole in NGC 3783. *Astrophysical J.* 736, 103. doi:10.1088/0004-637X/736/2/103

Brewer, B. J., Treu, T., Pancoast, A., Barth, A. J., Bennert, V. N., Bentz, M. C., et al. (2011). The mass of the black hole in arp 151 from bayesian modeling of reverberation mapping data. *Astrophysical J.* 733, L33. doi:10.1088/2041-8205/733/2/L33

Buisson, D. J. K., Parker, M. L., Kara, E., Vasudevan, R. V., Lohfink, A. M., Pinto, C., et al. (2018). NuSTAR observations of Mrk 766: distinguishing reflection from absorption. *MNRAS* 480, 3689–3701. doi:10.1093/mnras/sty2081

Bustamante, S., and Springel, V. (2019). Spin evolution and feedback of supermassive black holes in cosmological simulations. *MNRAS* 490, 4133–4153. doi:10.1093/mnras/stz2836

Cackett, E. M., Chiang, C.-Y., McHardy, I., Edelson, R., Goad, M. R., Horne, K., et al. (2018). Accretion disk reverberation with hubble space telescope observations of NGC 4593: evidence for diffuse continuum lags. *Astrophysical J.* 857, 53. doi:10.3847/1538-4357/aab4f7

Carter, B. (1971). Axisymmetric black hole has only two degrees of freedom. *Phys. Rev. Lett.* 26, 331–333. doi:10.1103/PhysRevLett.26.331

Chamani, W., Koljonen, K., and Savolainen, T. (2020). Joint XMM-Newton and NuSTAR observations of the reflection spectrum of III Zw 2. *A&A* 635, A172. doi:10.1051/0004-6361/201936992

Choudhury, K., García, J. A., Steiner, J. F., and Bambi, C. (2017). Testing the performance and accuracy of the RELXILL model for the relativistic X-ray reflection from accretion disks. *Astrophysical J.* 851, 57. doi:10.3847/1538-4357/aa9925

Cicone, C., Maiolino, R., Sturm, E., Graciá-Carpio, J., Feruglio, C., Neri, R., et al. (2014). Massive molecular outflows and evidence for AGN feedback from CO observations. *A&A* 562, A21. doi:10.1051/0004-6361/201322464

Cole, S., Lacey, C. G., Baugh, C. M., and Frenk, C. S. (2000). Hierarchical galaxy formation. *MNRAS* 319, 168–204. doi:10.1046/j.1365-8711.2000.03879.x

Connors, R., Tomsick, J., Draghis, P., Coughenour, B., Shaw, A., Garcia, J., et al. (2023). *The high energy X-ray probe (HEX-P): probing accretion onto stellar mass black holes*. arXiv e-prints , arXiv:2311.04782.

Crain, R. A., and van de Voort, F. (2023). Hydrodynamical simulations of the galaxy population: enduring successes and outstanding challenges. *ARA&A* 61, 473–515. doi:10.1146/annurev-astro-041923-043618

Croton, D. J., Springel, V., White, S. D. M., De Lucia, G., Frenk, C. S., Gao, L., et al. (2006). The many lives of active galactic nuclei: cooling flows, black holes and the luminosities and colours of galaxies. *MNRAS* 365, 11–28. doi:10.1111/j.1365-2966.2005.09675.x

Curd, B., and Narayan, R. (2023). GRRMHD simulations of MAD accretion discs declining from super-Eddington to sub-Eddington accretion rates. *MNRAS* 518, 3441–3461. doi:10.1093/mnras/stac3330

Dauser, T., García, J., Parker, M. L., Fabian, A. C., and Wilms, J. (2014). The role of the reflection fraction in constraining black hole spin. *MNRAS* 444, L100–L104. doi:10.1093/mnrasl/slu125

Dauser, T., García, J., and Wilms, J. (2016). Relativistic reflection: review and recent developments in modeling. *Astron. Nachrichten* 337, 362–367. doi:10.1002/asna.201612314

Dauser, T., Wilms, J., Reynolds, C. S., and Brenneman, L. W. (2010). Broad emission lines for a negatively spinning black hole. *MNRAS* 409, 1534–1540. doi:10.1111/j.1365-2966.2010.17393.x

Debattista, V. P., Mayer, L., Carollo, C. M., Moore, B., Wadsley, J., and Quinn, T. (2006). The secular evolution of disk structural parameters. *Astrophysical J.* 645, 209–227. doi:10.1086/504147

de La Calle Pérez, I., Longinotti, A. L., Guainazzi, M., Bianchi, S., Dovčiak, M., Cappi, M., et al. (2010). FERO: finding extreme relativistic objects. I. Statistics of relativistic Fe K_α lines in radio-quiet Type 1 AGN. *A&A* 524, A50. doi:10.1051/0004-6361/200913798

De Marco, B., Ponti, G., Cappi, M., Dadina, M., Uttley, P., Cackett, E. M., et al. (2013). Discovery of a relation between black hole mass and soft X-ray time lags in active galactic nuclei. *MNRAS* 431, 2441–2452. doi:10.1093/mnras/stt339

Di Matteo, T., Springel, V., and Hernquist, L. (2005). Energy input from quasars regulates the growth and activity of black holes and their host galaxies. *Nat* 433, 604–607. doi:10.1038/nature03335

Dotti, M., Colpi, M., Pallini, S., Perego, A., and Volonteri, M. (2013). On the orientation and magnitude of the black hole spin in galactic nuclei. *Astrophysical J.* 762, 68. doi:10.1088/0004-637X/762/2/68

Draghis, P. A., Miller, J. M., Zoghbi, A., Reynolds, M., Costantini, E., Gallo, L. C., et al. (2023). A systematic view of ten new black hole spins. *Astrophysical J.* 946, 19. doi:10.3847/1538-4357/acafe7

Dubois, Y., Beckmann, R., Bournaud, F., Choi, H., Devriendt, J., Jackson, R., et al. (2021). Introducing the NEWHORIZON simulation: galaxy properties with resolved internal dynamics across cosmic time. *A&A* 651, A109. doi:10.1051/0004-6361/202039429

Dubois, Y., Peirani, S., Pichon, C., Devriendt, J., Gavazzi, R., Welker, C., et al. (2016). The HORIZON-AGN simulation: morphological diversity of galaxies promoted by AGN feedback. *MNRAS* 463, 3948–3964. doi:10.1093/mnras/stw2265

Dubois, Y., Pichon, C., Welker, C., Le Borgne, D., Devriendt, J., Laigle, C., et al. (2014a). Dancing in the dark: galactic properties trace spin swings along the cosmic web. *MNRAS* 444, 1453–1468. doi:10.1093/mnras/stu1227

Dubois, Y., Volonteri, M., and Silk, J. (2014b). Black hole evolution - III. Statistical properties of mass growth and spin evolution using large-scale hydrodynamical cosmological simulations. *MNRAS* 440, 1590–1606. doi:10.1093/mnras/stu373

Dubois, Y., Volonteri, M., Silk, J., Devriendt, J., and Slyz, A. (2014c). Black hole evolution - II. Spinning black holes in a supernova-driven turbulent interstellar medium. *MNRAS* 440, 2333–2346. doi:10.1093/mnras/stu425

Duro, R., Dauser, T., Wilms, J., Pottschmidt, K., Nowak, M. A., Fritz, S., et al. (2011). The broad iron Kα line of Cygnus X-1 as seen by XMM-Newton in the EPIC-pn modified timing mode. *A&A* 533, L3. doi:10.1051/0004-6361/201117446

Edelson, R., Gelbord, J., Cackett, E., Peterson, B. M., Horne, K., Barth, A. J., et al. (2019). The first Swift intensive AGN accretion disk reverberation mapping survey. *Astrophysical J.* 870, 123. doi:10.3847/1538-4357/aaf3b4

Eraerds, T., Antonelli, V., Davis, C., Hall, D., Hetherington, O., Holland, A., et al. (2021). Enhanced simulations on the athena/wide field imager instrumental background. *J. Astronomical Telesc. Instrum. Syst.* 7, 034001. doi:10.1117/1.JATIS.7.3.034001

Esin, A. A., McClintock, J. E., and Narayan, R. (1997). Advection-dominated accretion and the spectral states of black hole X-ray binaries: application to nova muscae 1991. *Astrophysical J.* 489, 865–889. doi:10.1086/304829

Event Horizon Telescope Collaboration, Akiyama, K., Alberdi, A., Alef, W., Asada, K., Azulay, R., et al. (2019). First M87 event horizon telescope results. I. The shadow of the supermassive black hole. *Astrophysical J.* 875, L1. doi:10.3847/2041-8213/ab0ec7

Event Horizon Telescope Collaboration, Akiyama, K., Alberdi, A., Alef, W., Algaba, J. C., Anantua, R., et al. (2022). First Sagittarius A $\ast$ event horizon telescope results. I. The shadow of the supermassive black hole in the center of the Milky way. *Astrophysical J.* 930, L12. doi:10.3847/2041-8213/ac6674

Fabian, A. C. (2012). Observational evidence of active galactic nuclei feedback. *ARA&A* 50, 455–489. doi:10.1146/annurev-astro-081811-125521

Fabian, A. C., and Iwasawa, K. (1999). The mass density in black holes inferred from the X-ray background. *MNRAS* 303, L34–L36. doi:10.1046/j.1365-8711.1999.02404.x

Fabian, A. C., Iwasawa, K., Reynolds, C. S., and Young, A. J. (2000). Broad iron lines in active galactic nuclei. *PASP* 112, 1145–1161. doi:10.1086/316610

Fabian, A. C., Lohfink, A., Kara, E., Parker, M. L., Vasudevan, R., and Reynolds, C. S. (2015). Properties of AGN coronae in the NuSTAR era. *MNRAS* 451, 4375–4383. doi:10.1093/mnras/stv1218

Fabian, A. C., Rees, M. J., Stella, L., and White, N. E. (1989). X-ray fluorescence from the inner disc in Cygnus X-1. *MNRAS* 238, 729–736. doi:10.1093/mnras/238.3.729

Fabian, A. C., Zoghbi, A., Ross, R. R., Uttley, P., Gallo, L. C., Brandt, W. N., et al. (2009). Broad line emission from iron K- and L-shell transitions in the active galaxy 1H0707-495. *Nat* 459, 540–542. doi:10.1038/nature08007

Faucher-Giguère, C.-A., and Quataert, E. (2012). The physics of galactic winds driven by active galactic nuclei. *MNRAS* 425, 605–622. doi:10.1111/j.1365-2966.2012.21512.x

Fausnaugh, M. M., Denney, K. D., Barth, A. J., Bentz, M. C., Bottorff, M. C., Carini, M. T., et al. (2016). Space telescope and optical reverberation mapping project. III. Optical continuum emission and broadband time delays in NGC 5548. *Astrophysical J.* 821, 56. doi:10.3847/0004-637X/821/1/56

Ferrarese, L., and Merritt, D. (2000). A fundamental relation between supermassive black holes and their host galaxies. *Astrophysical JournalL* 539, L9–L12. doi:10.1086/312838

Feruglio, C., Maiolino, R., Piconcelli, E., Menci, N., Aussel, H., Lamastra, A., et al. (2010). Quasar feedback revealed by giant molecular outflows. *A&A* 518, L155. doi:10.1051/0004-6361/201015164

Fiacconi, D., Sijacki, D., and Pringle, J. E. (2018). Galactic nuclei evolution with spinning black holes: method and implementation. *MNRAS* 477, 3807–3835. doi:10.1093/mnras/sty893

Fiore, F., Feruglio, C., Shankar, F., Bischetti, M., Bongiorno, A., Brusa, M., et al. (2017). AGN wind scaling relations and the co-evolution of black holes and galaxies. *A&A* 601, A143. doi:10.1051/0004-6361/201629478

Gallo, L. C., Miniutti, G., Miller, J. M., Brenneman, L. W., Fabian, A. C., Guainazzi, M., et al. (2011). Multi-epoch X-ray observations of the Seyfert 1.2 galaxy Mrk 79: bulk motion of the illuminating X-ray source. *MNRAS* 411, 607–619. doi:10.1111/j.1365-2966.2010.17705.x

García, J., Dauser, T., Lohfink, A., Kallman, T. R., Steiner, J. F., McClintock, J. E., et al. (2014). Improved reflection models of black hole accretion disks: treating the angular distribution of X-rays. *Astrophysical J.* 782, 76. doi:10.1088/0004-637X/782/2/76

García, J., and Kallman, T. R. (2010). X-Ray reflected spectra from accretion disk models. I. Constant density atmospheres. *Astrophysical J.* 718, 695–706. doi:10.1088/0004-637X/718/2/695

García, J. A., Kara, E., Walton, D., Beuchert, T., Dauser, T., Gatuzz, E., et al. (2019). Implications of the warm corona and relativistic reflection models for the soft excess in mrk 509. *Astrophysical J.* 871, 88. doi:10.3847/1538-4357/aaf739

García, J. A., Steiner, J. F., McClintock, J. E., Remillard, R. A., Grinberg, V., and Dauser, T. (2015). X-ray reflection spectroscopy of the black hole GX 339–4: exploring the hard state with unprecedented sensitivity. *Astrophysical J.* 813, 84. doi:10.1088/0004-637X/813/2/84

García-Burillo, S., Combes, F., Schinnerer, E., Boone, F., and Hunt, L. K. (2005). Molecular gas in NUclei of GAlaxies (NUGA): IV. Gravitational torques and AGN feeding. *A&A* 441, 1011–1030. doi:10.1051/0004-6361:20052900

Gardner, J. P., Mather, J. C., Abbott, R., Abell, J. S., Abernathy, M., Abney, F. E., et al. (2023). The James Webb space telescope mission. *PASP* 135, 068001. doi:10.1088/1538-3873/acd1b5

Gebhardt, K., Richstone, D., Kormendy, J., Lauer, T. R., Ajhar, E. A., Bender, R., et al. (2000). Axisymmetric, three-integral models of galaxies: a massive black hole in NGC 3379. *AJ* 119, 1157–1171. doi:10.1086/301240

Gehrels, N., Chincarini, G., Giommi, P., Mason, K. O., Nousek, J. A., Wells, A. A., et al. (2004). The*Swift*Gamma-ray Burst mission. *Astrophysical J.* 611, 1005–1020. doi:10.1086/422091

Genzel, R., Eisenhauer, F., and Gillessen, S. (2010). The Galactic Center massive black hole and nuclear star cluster. *Rev. Mod. Phys.* 82, 3121–3195. doi:10.1103/RevModPhys.82.3121

George, I. M., and Fabian, A. C. (1991). X-ray reflection from cold matter in active galactic nuclei and X-ray binaries. *MNRAS* 249, 352–367. doi:10.1093/mnras/249.2.352

Ghez, A. M., Klein, B. L., Morris, M., and Becklin, E. E. (1998). High proper-motion stars in the vicinity of Sagittarius A ∗ : evidence for a supermassive black hole at the center of our galaxy. *Astrophysical J.* 509, 678–686. doi:10.1086/306528

Ghez, A. M., Salim, S., Weinberg, N. N., Lu, J. R., Do, T., Dunn, J. K., et al. (2008). Measuring distance and properties of the Milky way's central supermassive black hole with stellar orbits. *Astrophysical J.* 689, 1044–1062. doi:10.1086/592738

Giustini, M., and Proga, D. (2019). A global view of the inner accretion and ejection flow around super massive black holes. Radiation-driven accretion disk winds in a physical context. *A&A* 630, A94. doi:10.1051/0004-6361/201833810

Gravity Collaboration, Abuter, R., Amorim, A., Anugu, N., Bauböck, M., Benisty, M., et al. (2018). Detection of the gravitational redshift in the orbit of the star S2 near the Galactic centre massive black hole. *A&A* 615, L15. doi:10.1051/0004-6361/201833718

GRAVITY Collaboration, Amorim, A., Brandner, W., Clénet, Y., Davies, R., de Zeeuw, P. T., et al. (2020). *The spatially resolved broad line region of IRAS 09149-6206*. arXiv e-prints , arXiv:2009.08463.

GRAVITY Collaboration, Amorim, A., Bauböck, M., Brandner, W., Bolzer, M., Clénet, Y., et al. (2021). The central parsec of NGC 3783: a rotating broad emission line region, asymmetric hot dust structure, and compact coronal line region. *A&A* 648, A117. doi:10.1051/0004-6361/202040061

Greene, J. E., and Ho, L. C. (2005). Estimating black hole masses in active galaxies using the Hα emission line. *Astrophysical J.* 630, 122–129. doi:10.1086/431897

Guo, W.-J., Li, Y.-R., Zhang, Z.-X., Ho, L. C., and Wang, J.-M. (2022). Accretion disk size measurements of active galactic nuclei monitored by the zwicky transient facility. *Astrophysical J.* 929, 19. doi:10.3847/1538-4357/ac4e84

Harikane, Y., Zhang, Y., Nakajima, K., Ouchi, M., Isobe, Y., Ono, Y., et al. (2023). *JWST/NIRSpec first census of broad-line AGNs at z=4-7: detection of 10 faint AGNs with M_BH˜106-107 M_sun and their host galaxy properties*. arXiv e-prints , arXiv:2303.11946.

Healy, J., Lousto, C. O., and Zlochower, Y. (2014). Remnant mass, spin, and recoil from spin aligned black-hole binaries. *Phys. Rev. D.* 90, 104004. doi:10.1103/PhysRevD.90.104004

Henriques, B. M. B., White, S. D. M., Lilly, S. J., Bell, E. F., Bluck, A. F. L., and Terrazas, B. A. (2019). The origin of the mass scales for maximal star formation efficiency and quenching: the critical role of supernovae. *MNRAS* 485, 3446–3456. doi:10.1093/mnras/stz577

Hlavacek-Larrondo, J., Fabian, A. C., Edge, A. C., Ebeling, H., Sanders, J. S., Hogan, M. T., et al. (2012). Extreme AGN feedback in the MAssive Cluster Survey: a detailed study of X-ray cavities at z ~0.3. *Mon. Notices R. Astronomical Soc.* 421, 1360–1384. doi:10.1111/j.1365-2966.2011.20405.x

Hlavacek-Larrondo, J., McDonald, M., Benson, B. A., Forman, W. R., Allen, S. W., Bleem, L. E., et al. (2015). X-ray cavities in a sample of 83 spt-selected clusters of galaxies: tracing the evolution of agn feedback in clusters of galaxies out to z = 1.2. *Astrophysical J.* 805, 35. doi:10.1088/0004-637X/805/1/35

Hofmann, F., Barausse, E., and Rezzolla, L. (2016). The final spin from binary black holes in quasi-circular orbits. *Astrophysical J.* 825, L19. doi:10.3847/2041-8205/825/2/L19

Homayouni, Y., Sturm, M. R., Trump, J. R., Horne, K., Grier, C. J., Shen, Y., et al. (2022). The sloan digital sky survey reverberation mapping project: UV-optical accretion disk measurements with the hubble space telescope. *Astrophysical J.* 926, 225. doi:10.3847/1538-4357/ac478b

Hopkins, P. F., Hernquist, L., Cox, T. J., Di Matteo, T., Robertson, B., and Springel, V. (2006). A unified, merger-driven model of the origin of starbursts, quasars, the cosmic X-ray background, supermassive black holes, and galaxy spheroids. *Astrophys. J. Suppl. S* 163, 1–49. doi:10.1086/499298

Hopkins, P. F., Kereš, D., Oñorbe, J., Faucher-Giguère, C.-A., Quataert, E., Murray, N., et al. (2014). Galaxies on FIRE (Feedback in Realistic Environments): stellar feedback explains cosmologically inefficient star formation. *MNRAS* 445, 581–603. doi:10.1093/mnras/stu1738

Hopkins, P. F., and Quataert, E. (2010). How do massive black holes get their gas? *MNRAS* 407, 1529–1564. doi:10.1111/j.1365-2966.2010.17064.x

Hopkins, P. F., Quataert, E., and Murray, N. (2011). Self-regulated star formation in galaxies via momentum input from massive stars. *MNRAS* 417, 950–973. doi:10.1111/j.1365-2966.2011.19306.x

Hoyle, F., and Lyttleton, R. A. (1939). The effect of interstellar matter on climatic variation. *Proc. Camb. Philosophical Soc.* 35, 405–415. doi:10.1017/S0305004100021150

Ingram, A., Mastroserio, G., van der Klis, M., Nathan, E., Connors, R., Dauser, T., et al. (2022). On measuring the Hubble constant with X-ray reverberation mapping of active galactic nuclei. *MNRAS* 509, 619–633. doi:10.1093/mnras/stab2950

Israel, W. (1967). Event horizons in static vacuum space-times. *Phys. Rev.* 164, 1776–1779. doi:10.1103/PhysRev.164.1776

Israel, W. (1968). Event horizons in static electrovac space-times. *Commun. Math. Phys.* 8, 245–260. doi:10.1007/BF01645859

Jiang, J., Buisson, D. J. K., Dauser, T., Fabian, A. C., Fürst, F., Gallo, L. C., et al. (2022). A NuSTAR and Swift view of the hard state of MAXI J1813-095. *MNRAS* 514, 1952–1960. doi:10.1093/mnras/stac1401

Jiang, J., Fabian, A. C., Dauser, T., Gallo, L., García, J. A., Kara, E., et al. (2019). High Density Reflection Spectroscopy - II. The density of the inner black hole accretion disc in AGN. *MNRAS* 489, 3436–3455. doi:10.1093/mnras/stz2326

Jiang, J., Parker, M. L., Fabian, A. C., Alston, W. N., Buisson, D. J. K., Cackett, E. M., et al. (2018). The 1.5 Ms observing campaign on IRAS 13224-3809 - I. X-ray spectral analysis. *MNRAS* 477, 3711–3726. doi:10.1093/mnras/sty836

Jiang, Y.-F., Green, P. J., Greene, J. E., Morganson, E., Shen, Y., Pancoast, A., et al. (2017). Detection of time lags between quasar continuum emission bands based on pan-STARRS light curves. *Astrophysical J.* 836, 186. doi:10.3847/1538-4357/aa5b91

Kammoun, E., Lohfink, A. M., Masterson, M., Wilkins, D. R., Zhao, X., Baloković, M., et al. (2023). *The High Energy X-ray Probe (HEX-P): probing the physics of the X-ray corona in active galactic nuclei. arXiv e-prints* arXiv:2311.04679. doi:10.3389/fspas.2023.1308056

Kammoun, E. S., Nardini, E., and Risaliti, G. (2018). Testing the accuracy of reflection-based supermassive black hole spin measurements in AGN. *A&A* 614, A44. doi:10.1051/0004-6361/201732377

Kara, E., Alston, W. N., Fabian, A. C., Cackett, E. M., Uttley, P., Reynolds, C. S., et al. (2016). A global look at X-ray time lags in Seyfert galaxies. *MNRAS* 462, 511–531. doi:10.1093/mnras/stw1695

Kara, E., Steiner, J. F., Fabian, A. C., Cackett, E. M., Uttley, P., Remillard, R. A., et al. (2019). The corona contracts in a black-hole transient. *Nat* 565, 198–201. doi:10.1038/s41586-018-0803-x

Katz, N., Weinberg, D. H., and Hernquist, L. (1996). Cosmological simulations with TreeSPH. *Astrophysical JournalS* 105, 19. doi:10.1086/192305

Kaviraj, S., Laigle, C., Kimm, T., Devriendt, J. E. G., Dubois, Y., Pichon, C., et al. (2017). The Horizon-AGN simulation: evolution of galaxy properties over cosmic time. *MNRAS* 467, stx126–4752. doi:10.1093/mnras/stx126

Kereš, D., Katz, N., Weinberg, D. H., and Davé, R. (2005). How do galaxies get their gas? *MNRAS* 363, 2–28. doi:10.1111/j.1365-2966.2005.09451.x

Kesden, M. (2008). Can binary mergers produce maximally spinning black holes? *Phys. Rev. D.* 78, 084030. doi:10.1103/PhysRevD.78.084030

King, A. L., Walton, D. J., Miller, J. M., Barret, D., Boggs, S. E., Christensen, F. E., et al. (2014). The disk wind in the rapidly spinning stellar-mass black hole 4U 1630-472 observed with NuSTAR. *Astrophysical J.* 784, L2. doi:10.1088/2041-8205/784/1/L2

King, A. R., Pringle, J. E., and Hofmann, J. A. (2008). The evolution of black hole mass and spin in active galactic nuclei. *MNRAS* 385, 1621–1627. doi:10.1111/j.1365-2966.2008.12943.x

Kollmeier, J., Anderson, S. F., Blanc, G. A., Blanton, M. R., Covey, K. R., Crane, J., et al. (2019). SDSS-V pioneering panoptic spectroscopy. *Bull. Am. Astronomical Soc.* 51, 274.

Komatsu, E., Smith, K. M., Dunkley, J., Bennett, C. L., Gold, B., Hinshaw, G., et al. (2011). Seven-year wilkinson microwave anisotropy probe (WMAP) observations: cosmological interpretation. *Astrophysical JournalS* 192, 18. doi:10.1088/0067-0049/192/2/18

Kormendy, J., Bender, R., Evans, A. S., and Richstone, D. (1998). The mass distribution in the elliptical galaxy NGC 3377: evidence for a 2 × 10[TSUP]8[/TSUP] [ITAL]M[/ITAL] [TINF] [sun] [/TINF] black hole. *AJ* 115, 1823–1839. doi:10.1086/300313

Kormendy, J., and Ho, L. C. (2013). Coevolution (or not) of supermassive black holes and host galaxies. *ARA&A* 51, 511–653. doi:10.1146/annurev-astro-082708-101811

Koss, M., Trakhtenbrot, B., Ricci, C., Lamperti, I., Oh, K., Berney, S., et al. (2017). BAT AGN spectroscopic survey. I. Spectral measurements, derived quantities, and AGN demographics. *Astrophysical J.* 850, 74. doi:10.3847/1538-4357/aa8ec9

Koss, M. J., Trakhtenbrot, B., Ricci, C., Oh, K., Bauer, F. E., Stern, D., et al. (2022). *VizieR online data catalog: BASS. XXV. DR2 stellar velocity dispersions (Koss+, 2022).* Strasbourg, France: VizieR Online Data Catalog.

Kuijken, K., and Merrifield, M. R. (1995). Establishing the connection between peanut-shaped bulges and galactic bars. *Astrophysical J.* 443, L13. doi:10.1086/187824

Laor, A. (1991). Line profiles from a disk around a rotating black hole. *Astrophysical J.* 376, 90–94. doi:10.1086/170257

Liska, M., Tchekhovskoy, A., Ingram, A., and van der Klis, M. (2019). Bardeen-Petterson alignment, jets, and magnetic truncation in GRMHD simulations of tilted thin accretion discs. *MNRAS* 487, 550–561. doi:10.1093/mnras/stz834

Lowell, B., Jacquemin-Ide, J., Tchekhovskoy, A., and Duncan, A. (2023). *Rapid black hole spin-down by thick magnetically arrested disks. arXiv e-prints* arXiv:2302.01351.

Madsen, K. K., García, J. A., Stern, D., Armini, R., Basso, S., Coutinho, D., et al. (2023). *The high energy X-ray probe (HEX-P): instrument and mission profile. arXiv e-prints* , arXiv:2312.04678.

Magdziarz, P., and Zdziarski, A. A. (1995). Angle-dependent Compton reflection of X-rays and gamma-rays. *MNRAS* 273, 837–848. doi:10.1093/mnras/273.3.837

Magorrian, J., Tremaine, S., Richstone, D., Bender, R., Bower, G., Dressler, A., et al. (1998). The demography of massive dark objects in galaxy centers. *AJ* 115, 2285–2305. doi:10.1086/300353

Maiolino, R., Gallerani, S., Neri, R., Cicone, C., Ferrara, A., Genzel, R., et al. (2012). Evidence of strong quasar feedback in the early Universe. *MNRAS* 425, L66–L70. doi:10.1111/j.1745-3933.2012.01303.x

Maiolino, R., Scholtz, J., Curtis-Lake, E., Carniani, S., Baker, W., de Graaff, A., et al. (2023a). *JADES. The diverse population of infant Black Holes at 4<z<11: merging, tiny, poor, but mighty. arXiv e-prin*ts , arXiv:2308.01230.

Maiolino, R., Scholtz, J., Witstok, J., Carniani, S., D'Eugenio, F., de Graaff, A., et al. (2023b). *A small and vigorous black hole in the early Universe. arXiv e*-prints , arXiv:2305.12492.

Mallick, L., Fabian, A. C., García, J. A., Tomsick, J. A., Parker, M. L., Dauser, T., et al. (2022). High-density disc reflection spectroscopy of low-mass active galactic nuclei. *MNRAS* 513, 4361–4379. doi:10.1093/mnras/stac990

Mallick, L., Wilkins, D. R., Alston, W. N., Markowitz, A., De Marco, B., Parker, M. L., et al. (2021). Discovery of soft and hard X-ray time lags in low-mass AGNs. *MNRAS* 503, 3775–3783. doi:10.1093/mnras/stab627

Marconi, A., Risaliti, G., Gilli, R., Hunt, L. K., Maiolino, R., and Salvati, M. (2004). Local supermassive black holes, relics of active galactic nuclei and the X-ray background. *MNRAS* 351, 169–185. doi:10.1111/j.1365-2966.2004.07765.x

Marinucci, A., Matt, G., Kara, E., Miniutti, G., Elvis, M., Arevalo, P., et al. (2014). Simultaneous NuSTAR and XMM-Newton 0.5-80 keV spectroscopy of the narrow-line Seyfert 1 galaxy SWIFT J2127.4+5654. *MNRAS* 440, 2347–2356. doi:10.1093/mnras/stu404

Massonneau, W., Volonteri, M., Dubois, Y., and Beckmann, R. S. (2023). How the super-Eddington regime regulates black hole growth in high-redshift galaxies. *A&A* 670, A180. doi:10.1051/0004-6361/202243170

McConnell, N. J., and Ma, C.-P. (2013). Revisiting the scaling relations of black hole masses and host galaxy properties. *Astrophysical J.* 764, 184. doi:10.1088/0004-637X/764/2/184

McKinney, J. C., Tchekhovskoy, A., and Blandford, R. D. (2012). General relativistic magnetohydrodynamic simulations of magnetically choked accretion flows around black holes. *Mon. Notices R. Astronomical Soc.* 423, 3083–3117. doi:10.1111/j.1365-2966.2012.21074.x

McNamara, B. R., Wise, M., Nulsen, P. E. J., David, L. P., Sarazin, C. L., Bautz, M., et al. (2000). [ITAL]Chandra[/ITAL] X-ray observations of the Hydra A cluster: an interaction between the radio source and the X-ray–emitting gas. *Astrophysical J.* 534, L135–L138. doi:10.1086/312662

Meidinger, N., Albrecht, S., Beitler, C., Bonholzer, M., Emberger, V., Frank, J., et al. (2020). "Development status of the wide field imager instrument for Athena," in *Space telescopes and instrumentation 2020: ultraviolet to gamma ray*. Editors J.-W. A. den Herder, S. Nikzad, and K. Nakazawa (Online-Only, California, CA: SPIE), 114440T. doi:10.1117/12.2560507

Merloni, A., and Fabian, A. C. (2001). Accretion disc coronae as magnetic reservoirs. *MNRAS* 321, 549–552. doi:10.1046/j.1365-8711.2001.04060.x

Michel, F. C. (1972). Accretion of matter by condensed objects. *Astrophysics Space Sci.* 15, 153–160. doi:10.1007/BF00649949

Miller, J. M., Reynolds, C. S., Fabian, A. C., Miniutti, G., and Gallo, L. C. (2009). Stellar-mass black hole spin constraints from disk reflection and continuum modeling. *Astrophysical J.* Melville, NY, United States: AIP Publishing 697, 900–912. doi:10.1088/0004-637X/697/1/900

Miniutti, G., Fabian, A. C., and Miller, J. M. (2004). The relativistic Fe emission line in XTE J1650-500 with BeppoSAX: evidence for black hole spin and light-bending effects? *MNRAS* 351, 466–472. doi:10.1111/j.1365-2966.2004.07794.x

Miniutti, G., Ponti, G., Dadina, M., Cappi, M., and Malaguti, G. (2007). IRAS 13197-1627 has them all: Compton-thin absorption, photoionized gas, thermal plasmas and a broad Fe line. *MNRAS* 375, 227–239. doi:10.1111/j.1365-2966.2006.11291.x

Moderski, R., and Sikora, M. (1996). On black hole evolution in active galactic nuclei. *MNRAS* 283, 854–864. doi:10.1093/mnras/283.3.854

Moderski, R., Sikora, M., and Lasota, J. P. (1998). On the spin paradigm and the radio dichotomy of quasars. *MNRAS* 301, 142–148. doi:10.1046/j.1365-8711.1998.02009.x

Murray, N., Chiang, J., Grossman, S. A., and Voit, G. M. (1995). Accretion disk winds from active galactic nuclei. *Astrophysical J.* 451, 498. doi:10.1086/176238

Nandra, K., Barret, D., Barcons, X., Fabian, A., den Herder, J.-W., Piro, L., et al. (2013). *The hot and energetic Universe: a white paper presenting the science theme motivating the Athena+ mission. arXiv e-prints* arXiv:1306.2307.

Narayan, R., Chael, A., Chatterjee, K., Ricarte, A., and Curd, B. (2022). Jets in magnetically arrested hot accretion flows: geometry, power, and black hole spin-down. *Mon. Notices R. Astronomical Soc.* 511, 3795–3813. doi:10.1093/mnras/stac285

Narayan, R., and Yi, I. (1994). Advection-dominated accretion: a self-similar solution. *Astrophysical J.* 428, L13. doi:10.1086/187381

Nardini, E., Fabian, A. C., Reis, R. C., and Walton, D. J. (2011). A reflection origin for the soft and hard X-ray excess of Ark 120. *MNRAS* 410, 1251–1261. doi:10.1111/j.1365-2966.2010.17518.x

Novikov, I. D., and Frolov, V. P. (1989). *Physics of black holes*. Dordrecht, Netherlands: Kluwer Academic.

Novikov, I. D., and Thorne, K. S. (1973). Astrophysics of black holes. *Black Holes Les. Astres Occlus*, 343–450.

Oh, K., Koss, M., Markwardt, C. B., Schawinski, K., Baumgartner, W. H., Barthelmy, S. D., et al. (2018). The 105-month swift-BAT all-sky hard X-ray survey. *Astrophysical JournalS* 235, 4. doi:10.3847/1538-4365/aaa7fd

Pancoast, A., Brewer, B. J., and Treu, T. (2014). Modelling reverberation mapping data - I. Improved geometric and dynamical models and comparison with cross-correlation results. *MNRAS* 445, 3055–3072. doi:10.1093/mnras/stu1809

Parker, M. L., Wilkins, D. R., Fabian, A. C., Grupe, D., Dauser, T., Matt, G., et al. (2014). The NuSTAR spectrum of Mrk 335: extreme relativistic effects within two gravitational radii of the event horizon? *MNRAS* 443, 1723–1732. doi:10.1093/mnras/stu1246

Penna, R. F., McKinney, J. C., Narayan, R., Tchekhovskoy, A., Shafee, R., and McClintock, J. E. (2010). Simulations of magnetized discs around black holes: effects of black hole spin, disc thickness and magnetic field geometry. *MNRAS* 408, 752–782. doi:10.1111/j.1365-2966.2010.17170.x

Peterson, B. M. (1993). Reverberation mapping of active galactic nuclei. *PASP* 105, 247. doi:10.1086/133140

Peterson, B. M., Ferrarese, L., Gilbert, K. M., Kaspi, S., Malkan, M. A., Maoz, D., et al. (2004). Central masses and broad-line region sizes of active galactic nuclei. II. A homogeneous analysis of a large reverberation-mapping database. *Astrophysical J.* 613, 682–699. doi:10.1086/423269

Piotrowska, J. M., Bluck, A. F. L., Maiolino, R., and Peng, Y. (2022). On the quenching of star formation in observed and simulated central galaxies: evidence for the role of integrated AGN feedback. *MNRAS* 512, 1052–1090. doi:10.1093/mnras/stab3673

Ponti, G., Papadakis, I., Bianchi, S., Guainazzi, M., Matt, G., Uttley, P., et al. (2012). CAIXA: a catalogue of AGN in the*XMM-Newton*archive: III. Excess variance analysis. *A&A* 542, A83. doi:10.1051/0004-6361/201118326

Putman, M. E., Peek, J. E. G., and Joung, M. R. (2012). Gaseous galaxy halos. *ARA&A* 50, 491–529. doi:10.1146/annurev-astro-081811-125612

Raimundo, S. I., Fabian, A. C., Vasudevan, R. V., Gandhi, P., and Wu, J. (2012). Can we measure the accretion efficiency of active galactic nuclei? *MNRAS* 419, 2529–2544. doi:10.1111/j.1365-2966.2011.19904.x

Reis, R. C., Fabian, A. C., Ross, R. R., and Miller, J. M. (2009). Determining the spin of two stellar-mass black holes from disc reflection signatures. *MNRAS* 395, 1257–1264. doi:10.1111/j.1365-2966.2009.14622.x

Reis, R. C., and Miller, J. M. (2013). On the size and location of the X-ray emitting coronae around black holes. *Astrophysical J.* 769, L7. doi:10.1088/2041-8205/769/1/L7

Reis, R. C., Reynolds, M. T., Miller, J. M., and Walton, D. J. (2014). Reflection from the strong gravity regime in a lensed quasar at redshift $z = 0.658$. *Nat* 507, 207–209. doi:10.1038/nature13031

Reynolds, C. S. (2021). Observational constraints on black hole spin. *ARA&A* 59, 117–154. doi:10.1146/annurev-astro-112420-035022

Reynolds, C. S., Brenneman, L. W., Lohfink, A. M., Trippe, M. L., Miller, J. M., Reis, R. C., et al. (2012). "Probing relativistic astrophysics around SMBHs: the Suzaku AGN spin survey," in *Suzaku 2011: exploring the X-ray Universe: suzaku and beyond*. Editors R. Petre, K. Mitsuda, and L. Angelini doi:10.1063/1.3696170

Reynolds, M. T., Walton, D. J., Miller, J. M., and Reis, R. C. (2014). A rapidly spinning black hole powers the einstein cross. *Astrophysical J.* 792, L19. doi:10.1088/2041-8205/792/1/L19

Rezzolla, L., Diener, P., Dorband, E. N., Pollney, D., Reisswig, C., Schnetter, E., et al. (2008). The final spin from the coalescence of aligned-spin black hole binaries. *Astrophysical J.* 674, L29–L32. doi:10.1086/528935

Ricci, C., Tazaki, F., Ueda, Y., Paltani, S., Boissay, R., and Terashima, Y. (2014). Suzaku observation of IRAS 00521-7054, a peculiar type-II AGN with a very broad feature at 6 keV. *Astrophysical J.* 795, 147. doi:10.1088/0004-637X/795/2/147

Ricci, C., Trakhtenbrot, B., Koss, M. J., Ueda, Y., Del Vecchio, I., Treister, E., et al. (2017). BAT AGN spectroscopic survey. V. X-ray properties of the Swift/BAT 70-month AGN catalog. *Astrophysical JournalS* 233, 17. doi:10.3847/1538-4365/aa96ad

Rigby, J., Perrin, M., McElwain, M., Kimble, R., Friedman, S., Lallo, M., et al. (2023). The science performance of JWST as characterized in commissioning. *PASP* 135, 048001. doi:10.1088/1538-3873/acb293

Risaliti, G., Harrison, F. A., Madsen, K. K., Walton, D. J., Boggs, S. E., Christensen, F. E., et al. (2013). A rapidly spinning supermassive black hole at the centre of NGC1365. *Nat* 494, 449–451. doi:10.1038/nature11938

Ross, R. R., and Fabian, A. C. (2005). A comprehensive range of X-ray ionized-reflection models. *MNRAS* 358, 211–216. doi:10.1111/j.1365-2966.2005.08797.x

Russell, H. R., Fabian, A. C., McNamara, B. R., and Broderick, A. E. (2015). Inside the Bondi radius of M87. *MNRAS* 451, 588–600. doi:10.1093/mnras/stv954

Russell, H. R., Fabian, A. C., McNamara, B. R., Miller, J. M., Nulsen, P. E. J., Piotrowska, J. M., et al. (2018). The imprints of AGN feedback within a supermassive black hole's sphere of influence. *MNRAS* 477, 3583–3599. doi:10.1093/mnras/sty835

Saglia, R. P., Opitsch, M., Erwin, P., Thomas, J., Beifiori, A., Fabricius, M., et al. (2016). The SINFONI black hole survey: the black hole fundamental plane revisited and the paths of (Co)evolution of supermassive black holes and bulges. *Astrophysical J.* 818, 47. doi:10.3847/0004-637X/818/1/47

Sancisi, R., Fraternali, F., Oosterloo, T., and van der Hulst, T. (2008). Cold gas accretion in galaxies. *Astronomy Astrophysics Rev.* 15, 189–223. doi:10.1007/s00159-008-0010-0

Sanders, D. B., Soifer, B. T., Elias, J. H., Madore, B. F., Matthews, K., Neugebauer, G., et al. (1988). Ultraluminous infrared galaxies and the origin of quasars. *Astrophysical J.* 325, 74. doi:10.1086/165983

Schwarz, M. P. (1981). The response of gas in a galactic disk to bar forcing. *Astrophysical J.* 247, 77–88. doi:10.1086/159011

Sesana, A., Barausse, E., Dotti, M., and Rossi, E. M. (2014). Linking the spin evolution of massive black holes to galaxy kinematics. *Astrophysical J.* 794, 104. doi:10.1088/0004-637X/794/2/104

Shakura, N. I., and Sunyaev, R. A. (1973). Black holes in binary systems. Observational appearance. *A&A* 24, 337–355.

Shankar, F., Allevato, V., Bernardi, M., Marsden, C., Lapi, A., Menci, N., et al. (2020). Constraining black hole-galaxy scaling relations and radiative efficiency from galaxy clustering. *Nat. Astron.* 4, 282–291. doi:10.1038/s41550-019-0949-y

Shen, Y. (2013). The mass of quasars. *Bull. Astronomical Soc. India* 41, 61–115. doi:10.48550/arXiv.1302.2643

Sisk-Reynés, J., Reynolds, C. S., Matthews, J. H., and Smith, R. N. (2022). Evidence for a moderate spin from X-ray reflection of the high-mass supermassive black hole in the cluster-hosted quasar H1821+643. *MNRAS* 514, 2568–2580. doi:10.1093/mnras/stac1389

Soltan, A. (1982). Masses of quasars. *MNRAS* 200, 115–122. doi:10.1093/mnras/200.1.115

Springel, V. (2010). E pur si muove: galilean-invariant cosmological hydrodynamical simulations on a moving mesh. *MNRAS* 401, 791–851. doi:10.1111/j.1365-2966.2009.15715.x

Springel, V., Di Matteo, T., and Hernquist, L. (2005). Black holes in galaxy mergers: the formation of red elliptical galaxies. *Astrophysical J.* 620, L79–L82. doi:10.1086/428772

Steiner, J. F., McClintock, J. E., Remillard, R. A., Gou, L., Yamada, S., and Narayan, R. (2010). The constant inner-disk radius of LMC X-3: a basis for measuring black hole spin. *Astrophysical J.* 718, L117–L121. doi:10.1088/2041-8205/718/2/L117

Talbot, R. Y., Bourne, M. A., and Sijacki, D. (2021). Blandford-Znajek jets in galaxy formation simulations: method and implementation. *MNRAS* 504, 3619–3650. doi:10.1093/mnras/stab804

Talbot, R. Y., Sijacki, D., and Bourne, M. A. (2022). Blandford-Znajek jets in galaxy formation simulations: exploring the diversity of outflows produced by spin-driven AGN jets in Seyfert galaxies. *MNRAS* 514, 4535–4559. doi:10.1093/mnras/stac1566

Tanaka, Y., Nandra, K., Fabian, A. C., Inoue, H., Otani, C., Dotani, T., et al. (1995). Gravitationally redshifted emission implying an accretion disk and massive black hole in the active galaxy MCG-6-30-15. *Nat* 375, 659–661. doi:10.1038/375659a0

Tao, L., Tomsick, J. A., Qu, J., Zhang, S., Zhang, S., and Bu, Q. (2019). The spin of the black hole GRS 1716-249 determined from the hard intermediate state. *Astrophysical J.* 887, 184. doi:10.3847/1538-4357/ab5282

Tchekhovskoy, A., McKinney, J. C., and Narayan, R. (2012). General relativistic modeling of magnetized jets from accreting black holes. *J. Phys. Conf. Ser.* 372, 012040. doi:10.1088/1742-6596/372/1/012040

Tchekhovskoy, A., Narayan, R., and McKinney, J. C. (2011). Efficient generation of jets from magnetically arrested accretion on a rapidly spinning black hole. *MNRAS* 418, L79–L83. doi:10.1111/j.1745-3933.2011.01147.x

Terrazas, B. A., Bell, E. F., Henriques, B. M. B., White, S. D. M., Cattaneo, A., and Woo, J. (2016). Quiescence correlates strongly with directly measured black hole mass in central galaxies. *Astrophysical JournalL* 830, L12. doi:10.3847/2041-8205/830/1/L12

Teyssier, R. (2002). Cosmological hydrodynamics with adaptive mesh refinement. A new high resolution code called RAMSES. *A&A* 385, 337–364. doi:10.1051/0004-6361:20011817

Thorne, K. S. (1974). Disk-accretion onto a black hole. II. Evolution of the hole. *Astrophysical J.* 191, 507–520. doi:10.1086/152991

Tichy, W., and Marronetti, P. (2008). Final mass and spin of black-hole mergers. *Phys. Rev. D.* 78, 081501. doi:10.1103/PhysRevD.78.081501

Tomsick, J. A., Yamaoka, K., Corbel, S., Kaaret, P., Kalemci, E., and Migliari, S. (2009). Truncation of the inner accretion disk around a black hole at low luminosity. *Astrophysical J.* 707, L87–L91. doi:10.1088/0004-637X/707/1/L87

Toomre, A., and Toomre, J. (1972). Galactic bridges and tails. *Astrophysical J.* 178, 623–666. doi:10.1086/151823

Trakhtenbrot, B., and Netzer, H. (2012). Black hole growth to $z = 2$ - I. Improved virial methods for measuring M_{BH} and L/L_{Edd}. *MNRAS* 427, 3081–3102. doi:10.1111/j.1365-2966.2012.22056.x

Treves, A., and Turolla, R. (1999). Vacuum breakdown near a black hole charged by hypercritical accretion. *Astrophysical J.* 517, 396–398. doi:10.1086/307159

Tumlinson, J., Peeples, M. S., and Werk, J. K. (2017). The circumgalactic medium. *ARA&A* 55, 389–432. doi:10.1146/annurev-astro-091916-055240

Vestergaard, M. (2002). Determining central black hole masses in distant active galaxies. *Astrophysical J.* 571, 733–752. doi:10.1086/340045

Villar-Martín, M., Humphrey, A., Delgado, R. G., Colina, L., and Arribas, S. (2011). Ionized outflows in SDSS type 2 quasars at z - 0.3-0.6. *MNRAS* 418, 2032–2042. doi:10.1111/j.1365-2966.2011.19622.x

Vogelsberger, M., Marinacci, F., Torrey, P., and Puchwein, E. (2020). Cosmological simulations of galaxy formation. *Nat. Rev. Phys.* 2, 42–66. doi:10.1038/s42254-019-0127-2

Volonteri, M., Dubois, Y., Pichon, C., and Devriendt, J. (2016). The cosmic evolution of massive black holes in the Horizon-AGN simulation. *MNRAS* 460, 2979–2996. doi:10.1093/mnras/stw1123

Wald, R. M. (1984). *General relativity*. Chicago, IL, United States: the University of Chicago Press.

Walton, D. J., Alston, W. N., Kosec, P., Fabian, A. C., Gallo, L. C., Garcia, J. A., et al. (2020). A full characterization of the supermassive black hole in IRAS 09149-6206. *MNRAS* 499, 1480–1498. doi:10.1093/mnras/staa2961

Walton, D. J., Baloković, M., Fabian, A. C., Gallo, L. C., Koss, M., Nardini, E., et al. (2021). Extreme relativistic reflection in the active galaxy ESO 033-G002. *MNRAS* 506, 1557–1572. doi:10.1093/mnras/stab1290

Walton, D. J., Mooley, K., King, A. L., Tomsick, J. A., Miller, J. M., Dauser, T., et al. (2017). Living on a flare: relativistic reflection in V404 cyg observed by NuSTAR during its summer 2015 outburst. *Astrophysical J.* 839, 110. doi:10.3847/1538-4357/aa67e8

Walton, D. J., Nardini, E., Fabian, A. C., Gallo, L. C., and Reis, R. C. (2013). Suzaku observations of 'bare' active galactic nuclei. *MNRAS* 428, 2901–2920. doi:10.1093/mnras/sts227

Walton, D. J., Nardini, E., Gallo, L. C., Reynolds, M. T., Ricci, C., Dauser, T., et al. (2019). A low-flux state in IRAS 00521-7054 seen with NuSTAR and XMM-Newton: relativistic reflection and an ultrafast outflow. *MNRAS* 484, 2544–2555. doi:10.1093/mnras/stz115

Walton, D. J., Reis, R. C., Cackett, E. M., Fabian, A. C., and Miller, J. M. (2012). The similarity of broad iron lines in X-ray binaries and active galactic nuclei. *MNRAS* 422, 2510–2531. doi:10.1111/j.1365-2966.2012.20809.x

Walton, D. J., Risaliti, G., Harrison, F. A., Fabian, A. C., Miller, J. M., Arevalo, P., et al. (2014). NuSTAR and XMM-Newton observations of NGC 1365: extreme absorption variability and a constant inner accretion disk. *Astrophysical J.* 788, 76. doi:10.1088/0004-637X/788/1/76

Wang, J.-G., Dong, X.-B., Wang, T.-G., Ho, L. C., Yuan, W., Wang, H., et al. (2009). Estimating black hole masses in active galactic nuclei using the Mg II λ2800 emission line. *Astrophysical J.* 707, 1334–1346. doi:10.1088/0004-637X/707/2/1334

Weinberger, R., Springel, V., Hernquist, L., Pillepich, A., Marinacci, F., Pakmor, R., et al. (2017). Simulating galaxy formation with black hole driven thermal and kinetic feedback. *MNRAS* 465, 3291–3308. doi:10.1093/mnras/stw2944

Werner, N., McNamara, B. R., Churazov, E., and Scannapieco, E. (2019). Hot atmospheres, cold gas, AGN feedback and the evolution of early type galaxies: a topical perspective. *Space Sci. Rev.* 215, 5. doi:10.1007/s11214-018-0571-9

Wilkins, D. R., Gallo, L. C., Costantini, E., Brandt, W. N., and Blandford, R. D. (2022). Acceleration and cooling of the corona during X-ray flares from the Seyfert galaxy I Zw 1. *MNRAS* 512, 761–775. doi:10.1093/mnras/stac416

Wilkins, D. R., Gallo, L. C., Grupe, D., Bonson, K., Komossa, S., and Fabian, A. C. (2015). Flaring from the supermassive black hole in Mrk 335 studied with Swift and NuSTAR. *MNRAS* 454, 4440–4451. doi:10.1093/mnras/stv2130

Wong, K.-W., Irwin, J. A., Shcherbakov, R. V., Yukita, M., Million, E. T., and Bregman, J. N. (2014). The megasecond chandra X-ray visionary project observation of NGC 3115: witnessing the flow of hot gas within the Bondi radius. *Astrophysical J.* 780, 9. doi:10.1088/0004-637X/780/1/9

Wong, K.-W., Irwin, J. A., Yukita, M., Million, E. T., Mathews, W. G., and Bregman, J. N. (2011). Resolving the Bondi accretion flow toward the supermassive black hole of NGC 3115 with chandra. *Astrophysical J.* 736, L23. doi:10.1088/2041-8205/736/1/L23

Woo, J.-H., Yoon, Y., Park, S., Park, D., and Kim, S. C. (2015). The black hole mass-stellar velocity dispersion relation of narrow-line seyfert 1 galaxies. *Astrophysical J.* 801, 38. doi:10.1088/0004-637X/801/1/38

Xu, Y., Harrison, F. A., García, J. A., Fabian, A. C., Fürst, F., Gandhi, P., et al. (2018). Reflection spectra of the black hole binary candidate MAXI j1535-571 in the hard state observed by NuSTAR. *Astrophysical J.* 852, L34. doi:10.3847/2041-8213/aaa4b2

Yuan, F., and Narayan, R. (2014). Hot accretion flows around black holes. *ARA&A* 52, 529–588. doi:10.1146/annurev-astro-082812-141003

Zdziarski, A. A., Johnson, W. N., and Magdziarz, P. (1996). Broad-band γ-ray and X-ray spectra of NGC 4151 and their implications for physical processes and geometry. *MNRAS* 283, 193–206. doi:10.1093/mnras/283.1.193

Zycki, P. T., Done, C., and Smith, D. A. (1999). The 1989 May outburst of the soft X-ray transient GS 2023+338 (V404 Cyg). *MNRAS* 309, 561–575. doi:10.1046/j.1365-8711.1999.02885.x